THEORETICAL EFFECT OF YIELD AND BURST HEIGHT OF ATMOSPHERIC EXPLOSIONS ON RAYLEIGH WAVE AMPLITUDES

David G. Harkrider, et al

Teledyne Geotech
Alexandria, Virginia

14 Feburary 1973

.....contributing to man's
understanding of the environment world

AL-72-3

THEORETICAL EFFECT OF YIELD AND BURST HEIGHT OF ATMOSPHERIC EXPLOSIONS ON RAYLEIGH WAVE AMPLITUDES

BY

O.G. HARKRIDER, C.A. NEWTON and E.A. FLINN

SPONSORED BY
ADVANCED RESEARCH PROJECTS AGENCY

MONITORED BY
AIR FORCE OFFICE OF SCIENTIFIC RESEARCH

ARPA ORDER NO. 1357

14 FEBRUARY 1973

TELEDYNE GEOTECH
ALEXANORIA LABORATORIES

76R

UNCLASSIFIED

Security Classification

DOCUMENT CONTROL DATA - R & D

(Security classification of title, body of abstract and indexing annotation must be entered when the overall report is classified)

1. ORIGINATING ACTIVITY *(Corporate author)*
Teledyne Geotech
Alexandria, Virginia 22313

2a. REPORT SECURITY CLASSIFICATION
UNCLASSIFIED

2b. GROUP

3. REPORT TITLE
THEORETICAL EFFECT OF YIELD AND BURST HEIGHT OF ATMOSPHERIC EXPLOSIONS ON RAYLEIGH WAVE AMPLITUDES

4. DESCRIPTIVE NOTES *(Type of report and inclusive dates)*
Scientific Interim

5. AUTHOR(S) *(First name, middle initial, last name)*
D G Harkrider
C A Newton
E A Flinn

6. REPORT DATE
14 Feb 1973

7a. TOTAL NO. OF PAGES
~~74~~ 76

7b. NO. OF REFS
29

8a. CONTRACT OR GRANT NO
F44620-69-C-0082

b. PROJECT NO.
AO 1357

c.
62701D

d.

9a. ORIGINATOR'S REPORT NUMBER(S)
AL-72-3

9b. OTHER REPORT NO(S) *(Any other numbers that may be assigned this report)*
AFOSR - TR - 73 - 0517

10. DISTRIBUTION STATEMENT
Approved for public release; distribution unlimited.

11. SUPPLEMENTARY NOTES
TECH, OTHER

12. SPONSORING MILITARY ACTIVITY
Air Force Office of Scientific Research
1400 Wilson Boulevard NPG
Arlington, Virginia 22209

13. ABSTRACT

Theoretical seismograms for fundamental mode Rayleigh waves were calculated for atmospheric point sources over oceanic and over continental earth models, as recorded at an epicentral distance of 10,000 km. Yields were uniformly distributed over the range 1 kT to 10 MT, for source altitudes in the range 0.3 to 92.0 km. The earth structures used were those of Gutenberg and of Anderson and Toksoz. The source models were point mass-injection and energy-injection sources at altitude, as well as a distributed pressure pulse at the surface of the earth.

i

DD FORM 1473

Security Classification

14 KEY WORDS	LINK A		LINK B		LINK C	
	ROLE	WT	ROLE	WT	ROLE	WT
Atmospheric nuclear explosions Rayleigh waves						

THEORETICAL EFFECT OF YIELD AND BURST HEIGHT OF ATMOSPHERIC EXPLOSIONS ON RAYLEIGH WAVE AMPLITUDES

ALEXANDRIA LABORATORIES REPORT NO. AL-72-3

Effective Date of Contract:	1 March 1969
Contract Expiration Date:	31 March 1972
Amount of Contract Dollars:	$ 590,572
Program Code:	1F10
Contract Number:	F-44620-69-C-0082
ARPA Order No.:	1357
Principal Investigator:	Carl A. Newton
Period Covered:	1 March 1969 through 31 March 1972

TABLE OF CONTENTS

LIST OF FIGURES

LIST OF FIGURES (Cont'd.)

LIST OF TABLES

ABSTRACT

Theoretical seismograms for fundamental mode Rayleigh waves were calculated for atmospheric point sources over oceanic and over continental earth models, as recorded at an epicentral distance of 10,000 km. Yields were uniformly distributed over the range 1 kT to 10 MT, for source altitudes in the range 0.3 to 92.0 km. The earth structures used were those of Gutenberg and of Anderson and Toksöz. The source models were point mass-injection and energy-injection sources at altitude, as well as a distributed pressure pulse at the surface of the earth.

It was found that: (1) as far as Rayleigh wave excitation is concerned, the mass-injection and energy-injection sources are equivalent; (2) for low altitudes the Rayleigh wave excitation is independent of source type, but at intermediate altitudes the surface overpressure source predicts greater amplitudes than the other two source models; (3) for most altitudes, the energy coupling from the atmosphere into Rayleigh waves is more efficient for the continental earth structure than for the oceanic structure; (4) Rayleigh wave amplitude is more sensitive to yield than to burst height; (5) dependence of Rayleigh wave amplitude is less than the cube root relation for low-yield explosions at intermediate altitudes, but greater for high-yield explosions at near-surface altitudes; (6) spectral splitting ratios do not show a systematic variation with yield and burst height.

Symbols Not Defined in Text

g	Gravitational acceleration
σ_2	Isothermal Brunt frequency
α	Sound velocity
ω	Angular frequency
P_o	Ambient pressure at sea level
$P_s(D)$	Ambient pressure at source height
p_{ao}	Peak overpressure of 1 kT source at distance a_o
c	Phase velocity (ω/k)
k	Wave number
T_{as}	Positive phase duration
a_s	Scaling distance
ρ_o	Ambient density at sea level
$\rho_s(D)$	Ambient density at source height
w_o	Vertical surface displacement
γ	Attenuation coefficient
a_e	Earth radius
θ_e	Epicentral distance in degrees
A_R	Rayleigh wave medium response, continental structure
A_e	Rayleigh wave medium response, earth/atmosphere structure
A_σ	Rayleigh wave medium response, oceanic structure

INTRODUCTION

In this paper we calculate Rayleigh wave excitation at teleseismic distances for a variety of source models, earth structures, source yields, and burst heights, and study the variation of the Rayleigh wave spectrum and waveform with these parameters.

We used Harkrider's (1964a) computer code for calculating the far-field modal exditation of acoustic-gravity waves in an atmosphere consisting of isothermal layers overlying a rigid halfspace, and a similar code (Harkrider, 1964b) for calculating Rayleigh wave propagation in a layered solid/liquid halfspace underlying a vacuum. These two codes have been merged in order to model the coupling of atmospheric and seismic wave propagation and to calculate the generation of Rayleigh waves from a point source in the atmosphere, and the latter code was also used to model a pressure source distributed on the solid free surface.

It was found that the loading of the atmosphere on the solid earth affected the Rayleigh wave characteristics by only about 0.01%, i.e., the ratio of atmospheric to solid earth density.

Previous attempts to predict Rayleigh wave excitation by atmospheric sources were either oversimplified or else heuristic and ad hoc in nature. Toksöz and Ben-Menahem (1965) assumed a point source in a homogeneous liquid halfspace overlying a homogeneous solid halfspace; they made use of an equation of Cagniard (1962) and predicted that the effect of burst height on Rayleigh wave excitation should be negligible in this situation. Nickel and Whitaker (1971) used an ingenious synthesis technique to approximate a layered solid earth model. We discuss below the validity of the assumptions

involved in their technique.

Harkrider and Flinn (1970) described the formulation for a point mass-injection source within one layer of the atmosphere. In the work reported here we modified the codes Harkrider and Flinn used to include Pierce's (1968) energy-injection source as well as a distributed surface overpressure source.

The solutions to an expanding ring and an expanding disk surface load on an isotropic solid half space have been obtained by Gakenheimer and Miklowitz (1969), Gakenheimer (1969), and Gakenheimer (1971) among others. Rayleigh waves and body waves due to an atmosphere explosion modeled by an equivalent moving normal force applied to a multilayered half space have been formulated by Hudson (1969) and computed for an equivalent stationary point source at the free surface by Douglas et al. (1972).

The codes used in the present work are described by Kerr (1971). Source scaling was done by standard methods (Harkrider and Flinn, 1970). Two earth models were used in the present work: the Gutenberg continental model (which has a low-velocity zone; see Ben-Menahem and Harkrider, 1964, p. 2610) and the Anderson-Toksöz oceanic model (Harkrider and Anderson, 1966, p. 2970). Earth and atmospheric layering characteristics were as usual assumed to be invariant between source and receiver.

Calculations were made for a variety of yields and burst heights for both earth models and for all three source models. Waveforms and spectra were calculated for yields of 1 kT to 10 MT and burst heights of 0.3 to 80 km.

Energy injection source in the atmosphere

The formulation for Rayleigh waves generated by an explosion in a gravitating atmosphere coupled to the solid earth by a mass injection source was described by Harkrider and Flinn (1970). We have modified our calculations by using the Pierce energy injection source (Pierce, 1968 and Pierce et al., 1970) which was used by them to calculate acoustic-gravity waves from an explosion in the atmosphere.

For an energy source at (r, z) = (0, D) (z positive upward) in an infinite isothermal gravitating ideal gas, the outgoing time-transformed parcel pressure $\langle p_{p_s} \rangle$ can be written in integral form as

$$\langle p_{p_s} \rangle = 2\pi i\omega G_E e^{-\lambda(z-D)} \int_0^\infty \left(1 - \frac{g^2 k^2}{\omega^4}\right) \cdot \frac{e^{-i\bar{\nu}|z-D|}}{i\bar{\nu}} J_o(kr) k \, dk \qquad (1)$$

where

$$\lambda = \gamma g / 2\alpha^2$$

$$\bar{\nu}^2 = (\omega/\alpha)^2 - h_2 k^2 - \lambda^2$$

$$h_2 = 1 - \sigma_2^2/\omega^2$$

and

$$G_E = \frac{a_s p_{as}}{2\pi} \frac{\exp\,[-i\phi_e]}{(b_s^2 + \omega^2)}$$

$$p_{as} = p_{ao} \left[\frac{P_s(D)}{P_o}\right]$$

$$b_s = 1/T_{as}$$

$$\phi_e = 2 \tan^{-1}(\omega/b_s)$$

Following Harkrider and Flinn (1970), we find that

$$\Delta v_s = 4\pi k \frac{G_E}{\rho_s(D)} \tag{2}$$

$$\Delta p_s = o$$

and

$$[w_o]_{R_j} = \left(\frac{2}{\pi}\right)^{1/2} \int_{-\infty}^{\infty} \frac{p_{as} a_s k_j^{-1/2}}{(\omega^2 + b_s^2)} \frac{e^{-\hat{\gamma}(\omega) r}}{(a_e \sin\theta_e)^{1/2}} A_e \tag{3}$$

$$\cdot \frac{1}{\rho_s(D)} \left[\frac{p_p(D)}{\dot{w}_o}\right] \exp\left[i(\omega t - k_j r + 3\pi/4 - \phi_e\right] d\omega$$

where

$$A_e = \frac{-i[GN - LH]}{(\partial F_e/\partial k)_\omega}$$

$$F_e = [NK - IM] - \frac{c\tilde{A}_{21}}{\tilde{A}_{22}} [GN - LH]$$

$$\left[\frac{p_p(D)}{\dot{w}_o}\right] = - (\tilde{A}_s)_{21} + \frac{\tilde{A}_{21}}{\tilde{A}_{22}} (\tilde{A}_s)_{22}$$

$\tilde{A}_s$ is the atmosphere product matrix evaluated at the source altitude, and $\tilde{A}$ is the same product matrix evaluated at the top of the atmosphere. k_j is the j'th root of the Rayleigh wave dispersion equation.

It should be noted that substitution of equation (2) into the source relations of Harkrider (1964b) yields the same acoustic-gravity wave overpressure relations as those of Pierce et al. (1971).

Rayleigh wave displacements from sea-level overpressures

For the excitation of Rayleigh waves by an overpressure specified at sea level, we model the earth by a multilayered elastic halfspace with an optional layered gravitating liquid at the surface. We formulate the problem for an azimuthally symmetric overpressure source $[p_s(r,t)]$ applied to the surface of the earth model.

The Fourier time-transformed source

$$\langle p_s(r) \rangle = \int_{-\infty}^{\infty} [p_s(r,t)] e^{-i\omega t} \, dt$$

can because of symmetry be written as

$$\langle p_s(r) \rangle = \int_0^\infty p_s \, J_o(kr) \, dk \tag{4}$$

where

$$p_s = k \int_0^\infty \langle p_s(r) \rangle \, J_o(kr) r \, dr$$

The twice transformed pressures and particle velocities at the free surface of the liquid layer for the oceanic model are related to those on the ocean bottom by

$$\begin{bmatrix} -\dot{w}_s \\ p_s \end{bmatrix} = \underline{A} \begin{bmatrix} -\dot{w}_o \\ p_o \end{bmatrix}$$

or

$$p_s = \left[-A_{21} + \frac{p_o}{\dot{w}_o} A_{22} \right] \dot{w}_o \tag{5}$$

where the ocean layer matrix A can be obtained from Dorman (1962) or by setting the gravitational acceleration equal to zero in the atmospheric matrices of Press and Harkrider (1962) and Harkrider and Flinn (1970).

If we assume the separable form of equation (4), the normal stress σ_o and the vertical (positive downward) displacement w_o at the ocean-solid earth interface are related to the elastic properties of the solid earth by

$$\left[\frac{\sigma_o}{\dot{w}_o/c}\right] = - \frac{[NK - LM]}{[GN - LH]} \tag{6}$$

where the quantities N, K, L, M, G, and H are defined by Harkrider (1964a, 1970). Assuming continuity of normal stress and vertical particle velocity at the liquid-solid interface we obtain by combining equations (5) and (6):

$$w_o = - i \frac{p_s}{k} \frac{1}{A_{22}} \frac{[GN - LH]}{F_\sigma} \tag{7}$$

where

$$F_\sigma = [NK - LM] - c \frac{A_{21}}{A_{22}} [GN - LH]$$

$$\dot{w}_o = i\omega w_o \qquad \text{and} \qquad p_o = - \sigma_o$$

Therefore the time-transformed vertical displacement on the ocean bottom

$$< w_o > = \int_o^\infty w_o J_o(kr)\, dk$$

is given by

$$\langle w_o \rangle = -i \int_o^\infty \frac{P_s}{k} \frac{1}{A_{22}} \frac{[GN - LH]}{F_\sigma} J_o(kr)\, dk \qquad (8)$$

For the overpressures applied to the surface of the continental model, the result is similar to the oceanic model:

$$\langle w_o \rangle = -i \int_o^\infty \frac{P_s}{k} \frac{[GN - LH]}{F_R} J_o(kr)\, dk \qquad (9)$$

where

$$F_R = [NK - LM]$$

This result could also be obtained by letting the thickness of the water layer approach zero in equation (8), since $A_{22} \rightarrow 1$ and $A_{21} \rightarrow 0$ in this limit.

Evaluating the residue contribution of integrals (8) and (9), we obtain the solutions for the vertical displacement spectra associated with the j'th mode Rayleigh waves. For the oceanic model the solution is

$$\{w_o\}_j = -\frac{\pi}{k_j} \frac{P_s}{A_{22}} \frac{[GN - LH]}{(\partial F_\sigma / \partial k)_j} H_o^{(2)}(k_j r) \qquad (10)$$

and for the continental model

$$\{ w_o \}_j = - \frac{\pi}{k_j} p_s \frac{[GN - LH]}{(\partial F_R / \partial k)_j} H_o^{(2)} (k_j r) \tag{11}$$

where k_j is the j'th root of the Rayleigh wave dispersion equation for the ocean:

$$F_\sigma(k_j, \omega) = 0$$

or the continent:

$$F_R(k_j, \omega) = 0$$

Although we restricted the problem to azimuthal symmetry, the solutions for more general source geometries will contain the quantities which depend only on the vertical properties of the medium as k_j, [GN - LH], and $(\partial F/\partial k)$. In particular, if the source can be represented as

$$\langle p_s(r,\theta) \rangle = \cos(m\theta) \int_o^\infty p_s \, J_m(kr) \, dk$$

the solution would be

$$\langle w_o(r,\theta) \rangle = -i \cos(m\theta) \int_o^\infty \frac{p_s}{k} \frac{1}{A_{22}} \frac{[GN - LH]}{F_\sigma} J_m(kr) \, dk$$

For more general pressure distributions on the earth's surface we can

integrate the solution for a point pressure source over the desired source area. The point pressure source is defined here as $p_s = k/2\pi$, in order that $\langle p_s(r) \rangle$ given in equation (4) be a delta function. Using equation (9), the solution for the point source is written

$$\langle w_o(r,\theta) \rangle = \frac{-i}{2\pi} \int_o^\infty \frac{[GN-LH]}{F_R} \; J_o(kr) \; dk$$

The solution for a distributed surface source, $\langle p_s(r,\theta) \rangle$, is then given by the integral over the surface S as

$$\langle w_o(r,\theta) \rangle = \int_S \langle p_s(r_o,\theta_o) \rangle \; G(\underset{\sim}{r} \,|\, \underset{\sim}{r}_o) \; dS_o$$

where we define

$$G(\underset{\sim}{r} \,|\, \underset{\sim}{r}_o) = \frac{-i}{2\pi} \int_o^\infty \frac{[GN - LH]}{F_R} \; J_o(kR) \; dk$$

$$R = |\underset{\sim}{r} - \underset{\sim}{r}_o|$$

and $\underset{\sim}{r}$ is the position vector in the (r, θ) plane. An example of this technique is given in Appendix A for a disc source, which can be verified by equation (4).

Surface overpressure models

The distributed sea level overpressures are assumed to result from a spherical wave incident at a rigid surface from a point source at a height D above the surface. The spherical wave front is assumed to expand with velocity α. That is, the overpressure at a distance r from ground

zero is

$$\langle p_s(r) \rangle = 2p_{os} \frac{e^{-i\omega R_o/\alpha}}{R_o}$$

where

$$R_o^2 = D^2 + r^2$$

The assumed pressure time history is the Glasstone pressure pulse (Glasstone, 1962):

$$[p_e(a_s,t)] = \begin{cases} p_{as}(1-\tau/T_{+as}) \exp[-\tau/T_{+as}], & \tau > o \\ o, & \tau < o \end{cases} \qquad (13)$$

where $\tau = t - a_s/\alpha$. p_{as} is the peak overpressure and T_{+as} is the positive phase duration at $R = a_s$. Expressing (13) as an outgoing spherical wave and taking the Fourier time transform, we obtain

$$\langle p_e(R_o) \rangle = \frac{ip_{as}a_s}{(\omega^2+b_s^2)R_o} \exp\{-i[\omega R_o/\alpha + 2\tan^{-1}(\omega/b_s)]\} \qquad (14)$$

where $b_s = 1/T_{+as}$. From equations (13) and (14) we see that

$$p_{os} = \frac{i\omega p_{as}a_s}{\omega^2+b_s^2} \exp[-i2\tan^{-1}(\omega/b_s)]$$

Using the Sommerfeld integral, we can express $\langle p_s(r) \rangle$ in the integral form of equation (4) as

$$\langle p_s(r) \rangle = -i2p_{os} \int_0^\infty \frac{e^{-i\nu D}}{\nu} \; k \; J_o(kr) \; dk$$

where

$$\nu^2 = \left(\frac{\omega}{\alpha}\right)^2 - k^2$$

and thus

$$p_s = \frac{2\omega p_{as} a_s k}{\nu(\omega^2 + b_s^2)} \exp\{-i[\nu D + 2 \tan^{-1}(\omega/b_s)]\} \tag{15}$$

We obtain the ocean bottom Rayleigh wave displacement in the far field by substituting equation (15) into equation (10) and transforming back into the time domain:

$$[w_o]_{R_j} = \left(\frac{2}{\pi}\right)^{1/2} \int_{-\infty}^{\infty} \frac{\omega p_{as} a_s k_j^{-1/2}}{A_{22}\nu(\omega^2 + b_s^2)} \frac{e^{-\hat{\gamma}(\omega) r}}{[a_e \sin \theta_e]^{1/2}} \; \mathbf{A}_\sigma \tag{16}$$

$$\bullet \exp\{i[\omega t - k_j r + 3\pi/4 - \phi_s]\} \, d\omega$$

where

$$\phi_s = \nu D + 2\tan^{-1}(\omega/b_s)$$

and

$$A_\sigma = -i \frac{[GN - LH]}{(\partial F_\sigma / \partial k)}$$

and where we have used the asymptotic expansion for large arguments of the Hankel function, as well as approximation for the earth's curvature, as in equation (3). The expression for the continental model can be obtained by setting $A_{22} = 1$ and $A_{21} = o$ in equation (16).

Source overpressure scaling

The scaling of the outgoing wave (equation 13) for the mass and energy injection source models for different yields and burst altitudes is done using the formulas in Glasstone (1962) Using values obtained from Glasstone (1957) for a 1 kT typical air-burst nuclear explosion, the scale distance a_s, peak overpressure p_{as}, and positive phase duration T_{+as} are given by:

$$a_s = \xi a_o \qquad p_{as} = \left[\frac{P_s(D)}{P_o}\right] p_{ao}$$

$$T_{+as} = \xi \left[\frac{\alpha_o}{\alpha}\right] T_{+ao} \qquad \xi = \left\{ W \left[\frac{P_o}{P_s(D)}\right] \right\}^{1/3}$$

Here, W is the kT equivalent yield, P_o and a_o are the ambient pressure and acoustic velocity at sea level, and P_s and a_s are at the burst altitude. Except for the low burst altitudes, this scaling at the source altitude is not appropriate for a surface applied source where we need the sea-level peak

overpressure, unlike Harkrider and Flinn (1970) where the scaling of the outgoing wave is done at the same altitude as the source.

For nuclear explosions in the intermediate altitude range, $10 \leq D \leq 100$ km, we use the weak shock overpressure relations derived by Murphy (1972):

$$p_{as}a_s = 0.2\ h\ [P_s(D)\ P_o]^{1/2}\ \frac{xe^x}{b(x)} \tag{17}$$

$$T_{+as} = .0857\ \frac{h}{\alpha}\ \frac{xb(x)}{(1 + x + n)}$$

$$b(x) = [1-2(1 + x + n)e^x E_1(x)]^{1/2}$$

where $E_1(x)$ is the exponential integral, h is the scale height of an exponential atmosphere, and x and n are matching parameters for a shock wave calculation in a spherically symmetric exponential atmosphere (Lutzky and Lehto, 1968). The matching parameters are given graphically and in tabular form as a function of σ_h in Murphy (1972). The parameter σ_h is a function of source height and yield:

$$\sigma_h = h\ \left[\frac{P_s(D)}{29.4\ W}\right]^{1/3}$$

where h is in km, $P_s(D)$ in millibars, and W in kT.

Equations (17) are the extrapolation relations using the Reed-Otterman analytic weak-shock theory (Reed, 1959). As in Murphy (1972), we will restrict our calculations to source heights and yields for which the ratio

of overpressure to ambient pressure on the ground is smaller than 0.1.

Isothermal atmosphere model

Since the result for the atmosphere/solid-earth system (equation 3) is similar to the distributed overpressure result (equation 16), we will compare the simple model of an isothermal gravitating atmosphere with the sea-level distributed source.

For a single-layer atmosphere of thickness H,

$$\tilde{A}_{21} = i\rho_o e^{-\lambda H} \frac{\delta}{\omega^3} \frac{\sin(\bar{\nu}H)}{\bar{\nu}}$$

$$\tilde{A}_{22} = e^{-\lambda H}[\cos(\bar{\nu}H) + f \sin(\bar{\nu}H)]$$

where

$$f = (\lambda - g/c^2)/\bar{\nu}$$

and

$$\delta = g^2k^2 - \omega^4$$

ρ_o is the sea level ambient density. The $\tilde{A}_s$ elements are identical to the above, with D replacing H.

Thus in equation (3) for the single layer system

$$\frac{1}{\rho_s(D)}\left[\frac{p_p(D)}{\dot{w}_o}\right] = ie^{2\lambda D}\ \frac{\delta}{\bar{\nu}\omega^3}\ \frac{\{[e^{i\Psi} - e^{-i\Psi}] + if\,[e^{i\Psi} + e^{-i\Psi}]\}}{e^{k\bar{\nu}H}[1 + e^{-2\bar{\nu}H} - if(1 - e^{-i2\bar{\nu}H})]}$$

where we have used the relations $\rho_s(D) = \rho_o e^{-2\lambda D}$ and $\Psi = \bar{\nu}(H-D)$.

Neglecting the exponential terms involving the height of the atmosphere, we have:

$$\frac{1}{\rho_s(D)}\left[\frac{p_p(D)}{\dot{w}_o}\right] \simeq \frac{P_o}{P_s(D)}\ \frac{\delta}{\bar{\nu}\omega^3}\ \exp\,[-i\bar{\nu}D + i2\tan^{-1}f]$$

For the range of frequencies and phase velocities associated with Rayleigh waves, the neglected exponential terms represent phase and group delays for waves which have travelled at least once to the top of the atmosphere. As H becomes larger, their contribution to the Rayleigh wave arrives increasingly later than the contribution of the direct wave from source to ground, which is represented in this approximation.

Harkrider and Flinn (1970) found that the atmosphere had little numerical effect on the medium response $\mathbf{A}_e$; i.e., for the ocean system, $\mathbf{A}_e \simeq \mathbf{A}_\sigma$ and for the continent $\mathbf{A}_e \simeq \mathbf{A}_R$. Thus, comparing equation (3) with the continent solution corresponding to equation (16), the integrands differ by a factor S_R for the surface and S_e for the energy injection source, where

$$S_R = p_{as}a_s\ \frac{e^{-\nu D}}{\nu} \qquad \text{and} \qquad S_e = p_{ao}a_s\ \frac{e^{-\bar{\nu}D}}{\bar{\nu}}\ e^{i2\tan^{-1}f}$$

after approximating δ in the Rayleigh wave (ω,k) range by

$$\delta = g^2k^2 - \omega^4 \simeq -\omega^4$$

For g = o the atmosphere is no longer exponential and we have f = o and $\overline{\nu} = \nu$. The two factors are now equal since p_{ao} and p_{as} differ only in the ratio of ambient pressures at the source altitude and sea level. If we use the energy injection source as our standard because of its success in acoustic gravity wave prediction, the correct applied overpressure, p_{as}, for equation (13) should be the sea level value, p_{ao}.

NUMERICAL RESULTS

Earth and atmosphere models

Two earth models were used throughout this study. The Gutenberg continental model was taken from Ben-Menahem and Harkrider (1964, p. 2610) and the Anderson-Toksöz oceanic model was taken from Harkrider and Anderson (1966, p. 2970). The velocities and densities of these models are shown in Figure 1.

The atmosphere was represented by isothermal layers comprising the standard ARDC atmosphere (Wares et al., 1960) and is extensively described by Press and Harkrider (1962) and Harkrider (1964). The temperature profile for the atmospheric model is shown in Figure 2. The velocities c and U, and the medium responses $\mathbf{A}_e$ for the atmosphere-continental model and for the atmosphere-oceanic model, as calculated by the atmosphere-earth coupled system dispersion program HASH, are tabulated in Table I.

Misleading values of Rayleigh dispersion for the coupled system are obtained when the Rayleigh wave roots

are apparently intersected by the roots of the atmospheric acoustic modes; these occur along lines of nearly infinite slope in this region of the velocity-period plane. Figure 3 shows the structure of the phase velocity curves at one such point of intersection, and Figure 4 shows the group velocities calculated for the roots shown in Figure 3. The normalized atmospheric eigen-function $\dot{w}_m/\dot{w}_o$ is additional evidence for this phenomenon: Figure 5 shows $\dot{w}_m/\dot{w}_o$ at period 41.875 seconds near a point of intersection, and T_{+1} and T_{-1} just 0.3125 seconds above and below T_o. The periods chosen for the Rayleigh wave synthesis described here were required to have appropriate kinetic energy densities in the bottom layer of the atmosphere. This criterion resulted in the best velocity and medium response values for our models. The group velocities for these chosen periods are listed in Table I.

Anelastic and scattering attenuation coefficient

The amplitude decay coefficients $\hat{\gamma}_A(\omega)$ used here were taken from a study by Alewine (1972). These values differ appreciably from those used in Harkrider and Flinn (1970), $\hat{\gamma}_{B-M}(\omega)$, which were obtained from a linear extrapolation of the long-period observations of Ben-Menahem (1965).

The $\hat{\gamma}_A(\omega)$ values are based on observations by Tryggvason and by Gutenberg and Richter (Alewine, 1972) for continental paths. We have used the $\hat{\gamma}_A(\omega)$ in the Rayleigh wave calculations for both continental and oceanic models. If other coefficients $\hat{\gamma}_o(\omega)$ are preferred, then the peak Rayleigh wave amplitudes reported here could be corrected by

$$\exp[\hat{\gamma}_A(\omega_m) - \hat{\gamma}_o(\omega_m)]\, r \qquad \text{where} \quad \omega_m = \frac{2\pi}{T_m}$$

and T_m is the period of the peak amplitude. If the spectral decay factor with the coefficients $\hat{\gamma}_o(\omega)$ causes the peak amplitude to occur at a different time within the Rayleigh wave train, corresponding to a different group arrival, then the best correction procedure (the only procedure if no wave form is given) is to redo the synthesis calculation.

As an illustration of these corrections we have calculated waveforms for a 100 kT energy injection source at an altitude of 18.6 km and epicentral distance of 10,000 km for $\hat{\gamma}_{B-M}(\omega)$, $\hat{\gamma}_A(\omega)$, and $\hat{\gamma}_o(\omega) = 0$. The spectral decay factors for a 10,000 km path are shown in Figure 6. We see in Figure 7 that the peak amplitudes for $\hat{\gamma}_A$ and $\hat{\gamma}$ occur at $T_m = 21$ sec, but for $\hat{\gamma}_{B-M}$ at $T_m = 46$ sec. Table II shows a comparison between the measured amplitudes and the amplitudes calculated by making corrections to the measured $\hat{\gamma}_A$ waveform.

The poor comparison at 21 sec for $\hat{\gamma}_o = 0$ (123 vs 173) might be the result of an anomalous Airy phase amplitude for this synthesis, since these comparisons were similar to those made for other source models. The peak amplitudes could also be calculated for different epicentral distances r' by multiplying the amplitude at distance r by

$$\exp\left[\hat{\gamma}(\omega_m)(r - r')\right]\left[\frac{r \sin(r/a_e)}{r' \sin(r'/a_e)}\right]^{1/2}$$

This correction is approximate and depends on the amount of dispersion of the wave train.

Results for low source altitudes

The theoretical seismograms presented by Harkrider and Flinn (1970) were recalculated to correct for a missing factor of $(2\pi)^{-1}$ and an incorrect altitude scaling for the ocean model. Examples of seismograms are shown in Figure 8 along with those calculated for the energy injection source (equation 3) and the analytical surface overpressure Glasstone source (equation 16). For these low source altitudes, as well as for higher ones, the seismograms for the point mass and energy sources are practically indistinguishable. We have chosen the energy source as the standard because it gives better results for the acoustic-gravity waves. Table III shows a comparison of the peak amplitudes for the various low altitude source models.

Intermediate source altitude results

For source altitudes in the range 10-1000 km and yields of 10, 100, and 1000 kT, we compared the Glasstone-scaled point energy source (equation 3) and the Murphy (1972) scaled surface overpressure source (equation 16).

Typical waveforms generated by these source models are shown in Figure 9. The smooth spectra for the surface source and the irregular-looking spectra for the source at altitude are predicted by the source terms in the integrands of the respective equations, and demonstrate the effect of multipathing in the atmosphere. The peak amplitudes for these source models, shown in Figure 10, are nearly the same for the lowest source altitudes, but at higher altitudes the modified Sachs scaling calculated by Murphy (1972) predicts a larger Rayleigh wave amplitude.

Uniform half space models

In 1971, Nickel and Whitaker presented a numerical technique in which the atmospheric explosion was modeled by a distributed source on the free surface of a solid half-space. The elastic constants of the homogeneous half-space were made to vary with the frequency in order to reproduce measured dispersion data. For a homogeneous half-space the medium response is given by Harkrider (1970) as

$$A_R = \frac{-r_\alpha^*}{4\rho V_R^3 \left\{ (\gamma-1) + \frac{\beta^2}{V_R^2}\frac{\gamma^2}{\alpha^2}\frac{[2V_R^2 - \alpha^2 - \beta^2]}{(\gamma-1)^2} \right\}} \omega$$

where $r_\alpha^* = -\left(1 - \frac{V_R^2}{\alpha^2}\right)^{1/2}$ and $\gamma = 2\frac{\beta^2}{V_R^2}$

Assuming a Poisson solid as in Nickel and Whitaker with the Lame' constants equal, then the observed phase velocity of Rayleigh waves $V_R(\omega)$ determines a frequency dependent shear, $\beta(\omega)$, and compressional velocity, $\alpha(\omega)$, given by

$$V_R = (2-2/\sqrt{3})\ \beta \qquad \text{and} \qquad \alpha = \sqrt{3}\ \beta$$

Thus the media response for this fictitious half-space can be determined to within a factor of ρ, the density, which is assumed to be independent of frequency or

$$\rho A_R \cong \frac{0.9745}{V_R(\omega)^3}\ \frac{1}{T} \times 10^{-11} \quad \text{microns}\ \frac{\text{sec}^2}{\text{cm}^4}$$

where V_R is in km/sec and T is in seconds. In figure 11, we show A_R for various earth structures including an oceanic model. If we assume a crustal density ρ between 2.50 and 3.0 there is good agreement between the vertically inhomogeneous media responses and the approximate half-space models of Nickel and Whitaker using our Rayleigh dispersion for a continent and ocean. This means that the technique of Nickel and Whitaker is valid for explosions over oceans as well as continents, a point questioned in Harkrider and Flinn (1970).

YIELD AND BURST HEIGHT DIAGNOSTICS

Analysis of theoretical seismograms to obtain a set of measurements capable of diagnosing yield and height of burst was attempted using the energy injection source model for both oceanic and continental layered structures. The peak amplitude, period of oscillation at the peak amplitude, and the surface wave magnitude were calculated, Table IV, at an epicentral distance of 10,000 km, yields of 1 kT to 10 MT, and burst altitudes to 80 km. Also the seismic coupling, defined by the ratio of seismic energy to explosive yield, E_s / W, where

$$\log E_s = 9.4 + 2.14\, M_s - 0.054\, M_s^2 \qquad \text{(Pomeroy, 1963)}$$

and

$$M_s = \log(A/T) + 1.66 \log\Delta - 0.18$$

A is peak-to-peak amplitude in mμ and Δ is epicentral distance in degrees. Figure 11 shows the relation of M_s to yield and burst height for the

continental and oceanic models. At most altitudes the continental M_s is greater than the oceanic M_s for a given yield; the exceptions are 10 km and 51.2 km. At a burst height of 80 km, both models show M_s proportional to $\frac{1}{2}$ logW; and near 0 km, M_s is proportional to logW. Figure 13 shows the relation of the maximum waveform amplitude (A_m) to yield and burst height for the two models. Except in the altitude range 40-60 km, the maximum amplitudes for the continental model are greater than the oceanic model amplitudes. If a measured quantity could be found with contours intersecting the contours shown in Figure 13 at angles approaching 90°, then we would be able to determine both yield and burst height from the Rayleigh wave. Without such a quantity we could determine the yield if the burst height is known, but knowing only the yield, the burst height cannot be determined uniquely.

If the yield and burst height are known for one of a series of explosions at the same location, then the yields for all others detonated at approximately the same altitude can be calculated by comparing the energy spectra. Figure 14 shows relative spectral energies, defined by

$$E_{R_N} = \frac{1}{N} \sum_{i=1}^{N} (A_i^2 / A_{R_i}^2)$$

where N is number of equally spaced spectral samples A_i, and the reference spectrum A_R is calculated from the theoretical waveform for an explosion of 1 kT at the same height and the same epicentral distance as the event with unknown yield. In terms of amplitudes rather than energies, the following conclusions can be drawn from Figure 14:

1. Cube root scaling is observed for the amplitude spectra of Rayleigh waves from high-altitude explosions over continental paths.

2. For intermediate altitudes, the amplitude spectra have a $W^{1/2}$ dependence for low yields and $W^{1/3}$ for high yields.

3. For near-surface altitudes, the amplitude spectra have a W dependence for high yields.

Further analysis revealed that when the amplitudes differ from cube root scaling, the shorter-period components are closer to the $W^{1/3}$ dependence than the longer period components. The quantity E_{R_n} was computed without smoothing the spectra A and A_R, but the scatter in our results might be removed by smoothing at least A_R.

We examined the amplitude spectral minima and the phase spectra to see if there existed a simple relationship to the burst height, but none could be found.

Spectral splitting, i.e., the ratio of energy in the longer-period end of the Rayleigh wave spectrum to energy in the shorter-period end, has been suggested as a discriminant between underground explosions and earthquakes (von Seggern and Lambert, 1970). The physical rationale is that the two source types should be sufficiently different in nature that the shape of the radiated elastic wave spectrum should be measurably different. Intuitively it seems reasonable that variations in yield and burst height of atmospheric explosions might produce similar effects, so we studied the spectral distribution of energy in the theoretical Rayleigh wave calculations.

We define the power spectral splitting ratio by

$$\langle R \rangle_T = \frac{P(T_2,T)}{P(T,T_1)} \quad , T_1 < T \leq T_2$$

Where $P(a,b) = \sum_{i=a}^{b} A_i^2$ and the A_i are the Fourier amplitude coefficients.

von Seggern and Lambert (1970) showed that the values of $\langle R \rangle_T$ obtained by splitting the spectra at T = 22 seconds separates the population of atmospheric explosion seismograms from earthquakes and underground explosion seismograms because the former contain less long-period energy than the latter. Putting T_1 = 10 seconds and T_2 = 62 seconds, we obtain the values of $\langle R \rangle_{22}$ shown in Figure 15 for the continental model. The only general relation we can conclude from these data is that for the higher burst altitudes there is a yield threshold above which $\langle R \rangle_{22}$ is constant. This relation is also observed in Figure 16, which gives $\langle R \rangle_T$ for T = 15, 20, 25, 30, and 40 seconds as a function of burst altitude for yields of 1, 10, and 10,000 kT. In another attempt to use $\langle R \rangle_T$ for yield and burst height diagnostics, we calculated the function

$$\tilde{R}(T) = \log [T^2 \langle R \rangle_T]$$

and we found that the shapes of $\tilde{R}(T)$ were nearly independent of the yield but were distinguishable for different burst heights. (Figure 17). Unfortunately there does not appear to be any systematic variation that would permit a burst height prediction from $\tilde{R}(T)$ when the source parameters are unknown.

CONCLUSIONS

Our theoretical treatment of Rayleigh waves generated by atmospheric nuclear explosions contains a number of approximations with regard to source spectra and scaling, the atmospheric model, and the earth model. Improvements in these assumptions will require comparisons with observations from sources

whose burst height and yield are known. The choice of peak overpressure scaling depends on such considerations.

Having analyzed our theoretical data base to find source diagnostics, we found that source yield may be estimated if the source altitude is approximately known. We expect the variation of yield to result in a continuous change of the waveforms and spectra. In the case of source altitude we are dealing with higher modes of the atmosphere system due to the large Rayleigh phase velocities compared to the acoustic velocities of the atmosphere. This means there are many nodal points in the atmosphere eigenfunction with respect to altitude and frequency. Since this eigenfunction is a factor in the source altitude term [see equation (3)] the variations in the altitude resulted in nearly discontinuous changes in spectra. We conclude that the yield diagnostics may not be useful for determining source altitude.

The seismic coupling is generally greater for explosions over continents than over oceans; the difference may be as much as 0.5 magnitude units. The major differences resulting from using different earth models are seen in the waveforms, which are governed largely by the group velocity dispersion. Since most travel paths are a combination of oceanic and continental segments, the effective dispersion will be a weighted average of the velocities used in computing these waveforms. The real earth paths will also cause changes in the amplitude spectra due to mode conversions and reflections where the structure is changing. In consideration of these effects (which we have not included in our analysis) we conclude that the best estimates of source altitude and yield will be made by comparing seismograms from explosions having common epicenters and travel paths such as the technique used by Toksöz and Ben-Menahem (1964).

REFERENCES

Aki, K., 1960, Study of earthquake mechanism by a method of phase equalization applied to Rayleigh and Love waves: J. Geophys. Res., 65, 729-740.

Alewine, R. W., 1972 (in press), Theoretical and observed distance corrections for Rayleigh wave magnitude: Bull. Seismol. Soc. Amer., 62.

Ben-Menahem, A. and Harkrider, D. G., 1964, Radiation patterns of seismic surface waves from buried dipolar point sources in a flat stratified earth: J. Geophys. Res., 69, 2605-2620.

Ben-Menahem, A., 1965, Observed attenuation and Q values of seismic surface waves in the upper mantle: J. Geophys. Res., 70, 4641-4652.

Cagniard, L., 1962, Reflection and refraction of progressive seismic waves, translated and revised by E. A. Flinn and C. H. Dix, McGraw-Hill Book Co., New York.

Dorman, J., 1962, Period equation for waves of Rayleigh type on a layered, liquid-solid half space: Bull. Seismol. Soc. Amer., 52, 389-397.

Douglas, A., Hudson, J. A. and Blamey, C., 1972, A quantitative evaluation of seismic signals of teleseismic distances - III, Computed P and Rayleigh wave seismograms: Geophys. J. R. astr. Soc., 28, 385-410.

Gakenheimer, D. C. and Miklowitz, J., 1969, Transient excitation of an elastic half space by a point load traveling on the surface: J. Appl. Mechanics, 36, 505-515.

Gakenheimer, D. C., 1969, Response of an elastic half space to an expanding ring of surface pressure: The RAND Corp., RM-6095-PR.

Gakenheimer, D. C., 1971, Response of an elastic half space to expanding surface loads: J. Appl. Mechanics, 38, 99-110.

Glasstone, S., ed., 1957 and 1962, The effects of nuclear weapons: U.S. Government Printing Office, Washington, D.C.

Harkrider, D. G., 1964a, Theoretical and observed acoustic-gravity waves from explosive sources in the atmosphere: J. Geophys. Res., 69, 5295-5321.

Harkrider, D. G., 1964b, Surface waves in multilayered elastic media, 1, Rayleigh and Love waves from buried sources in a multilayered elastic half-space: Bull. Seismol. Soc. Amer., 54, 627-679.

Harkrider, D. G., and Anderson, D. L., 1966, Surface wave energy from point sources in plane layered earth models: J. Geophys. Res., 71, 2967-2980.

Harkrider, D. G., 1970, Surface waves in multilayered elastic media, 2, Higher mode spectra and spectral ratios from point sources in plane layered earth models: Bull. Seismol. Soc. Amer., 60, 1937-1987.

Harkrider, D. G. and Flinn, A. E., 1970, Effect of crustal structure on Rayleigh waves generated by atmospheric explosions: Rev. Geophys., 8, 501-516.

Hudson, J. A., 1969, A quantitative evaluation of seismic signals at teleseismic distances - I, Radiation from point sources: Geophys. J. R. astr. Soc., 18, 233-249.

Kerr, A. U., Digital computer programs for recording and processing infrasonic array data: Geophys. J. R. astr. Soc., 26, 21-40.

Lutsky, M. and Lehto, D. L. 1968, Shock propagation in spherically symmetric exponential atmospheres: Phys. Fluids, 11, 1466-1472.

Murphy, Brian L., 1972, Variation of Rayleigh wave amplitude with yield and height of burst for intermediate-altitude nuclear detonations: J. Geophys. Res., 77, 808-817.

Nickel, G. H. and Whitaker, W. A., 1972, Distant seismic waves from a high-altitude source: Geophys. J. R. astr. Soc., 26, 369-378.

Pierce, A. D., 1968, Theoretical source models for the generation of acoustic-gravity waves by nuclear explosions, in Acoustic-Gravity Waves in the Atmosphere, T. M. Georges, ed., 9-24: U.S. Government Printing Office, Washington, D.C.

Pierce, A. D., Posey, J. W. and Iliff, E. F., 1971, Variation of nuclear explosion generated acoustic-gravity waveforms with burst height and with energy yield: J. Geophys. Res., 76, 5025-5042.

Pomeroy, P. W., 1963, Long-period seismic waves from large near-surface nuclear explosions: Bull. Seismol. Soc. Amer., 53, 109-150.

Press, F. and Harkrider, D. G., 1962, Propagation of acoustic-gravity waves in the atmosphere: J. Geophys. Res., 67, 3889-3908.

Reed, S. G., Jr., 1959, Note on finite amplitude propagation effects on shock wave travel times from explosions at high altitude: J. Acoust. Soc. Amer., 31, 1265.

Toksöz, M. N. and Ben-Menahem, A., 1964, Excitation of seismic surface waves by atmospheric nuclear explosions, J. Geophys. Res., 69, 1639-1648.

von Seggern, D., and Lambert, D. G., 1970, Theoretical and observed Rayleigh-wave spectra for explosions and earthquakes: J. Geophys. Res., 75, 1382-1402.

Wares, G. W., Champion, K. W., Pond, H. L., and Cole, A. E., 1960, Model atmosphere: in Handbook of Geophysics, 1-1, 1-37: The MacMillan Co., New York.

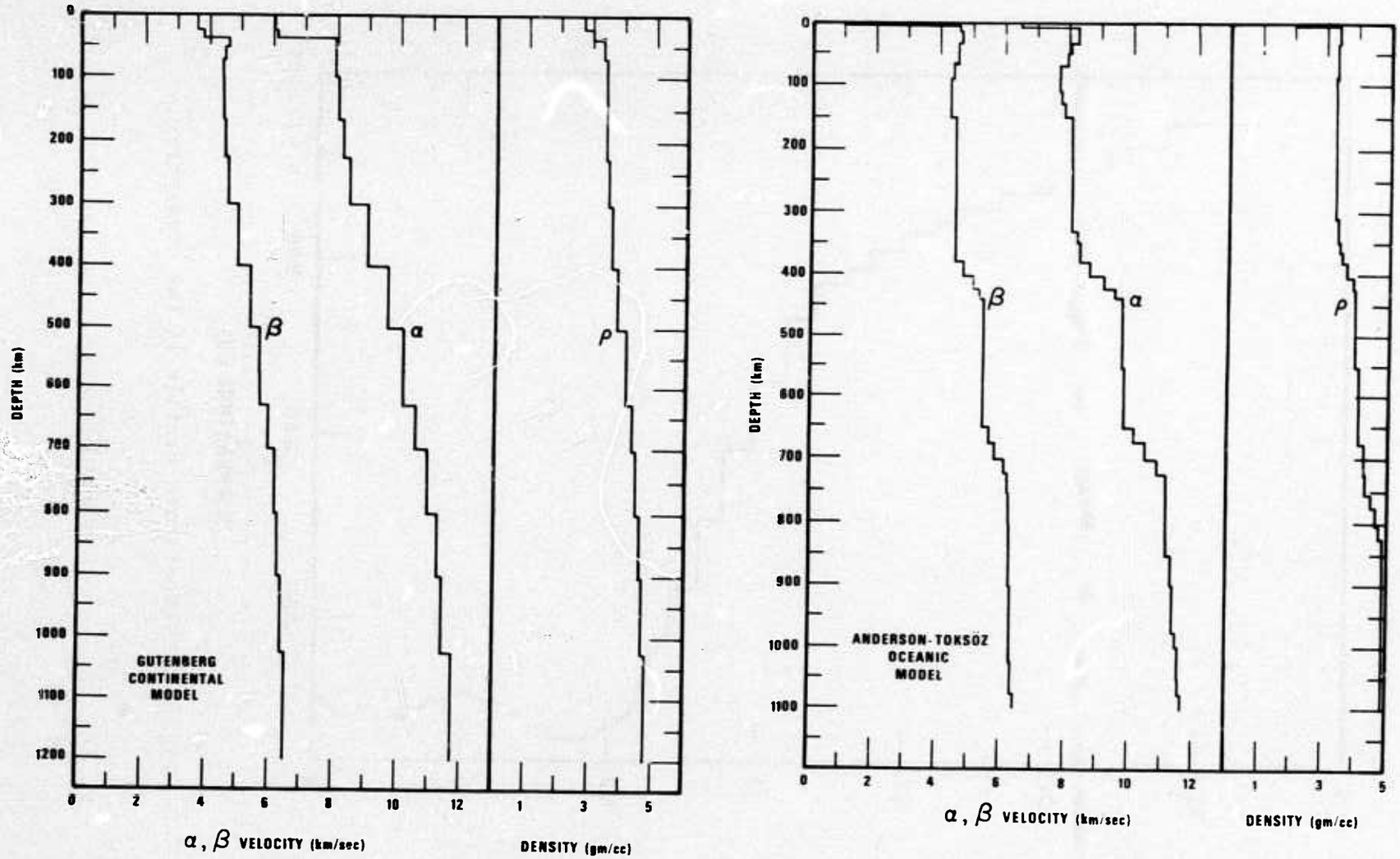

Figure 1. Velocity and density profiles for the continental and oceanic models in this work.

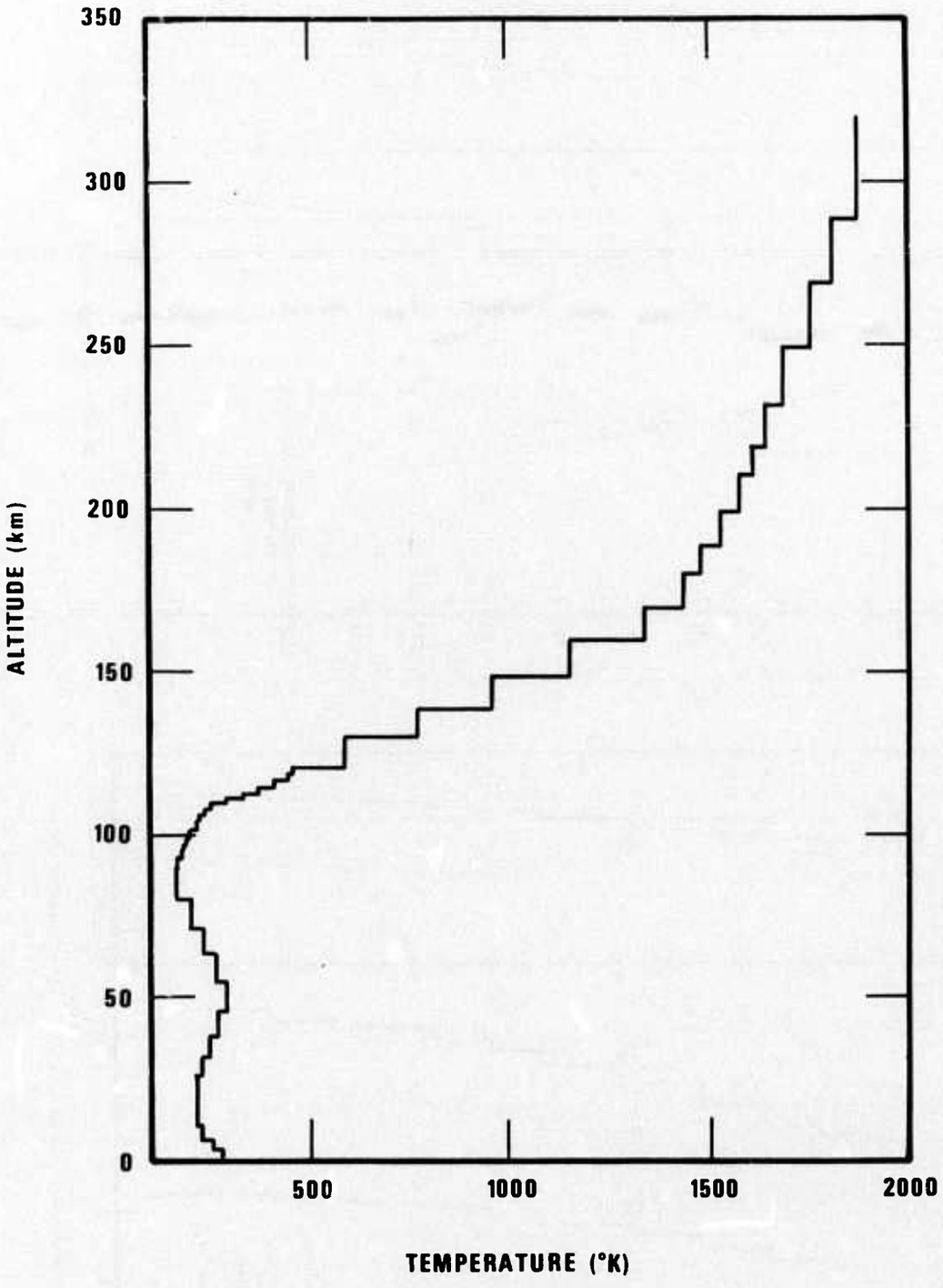

Figure 2. Temperature profile in the atmosphere.

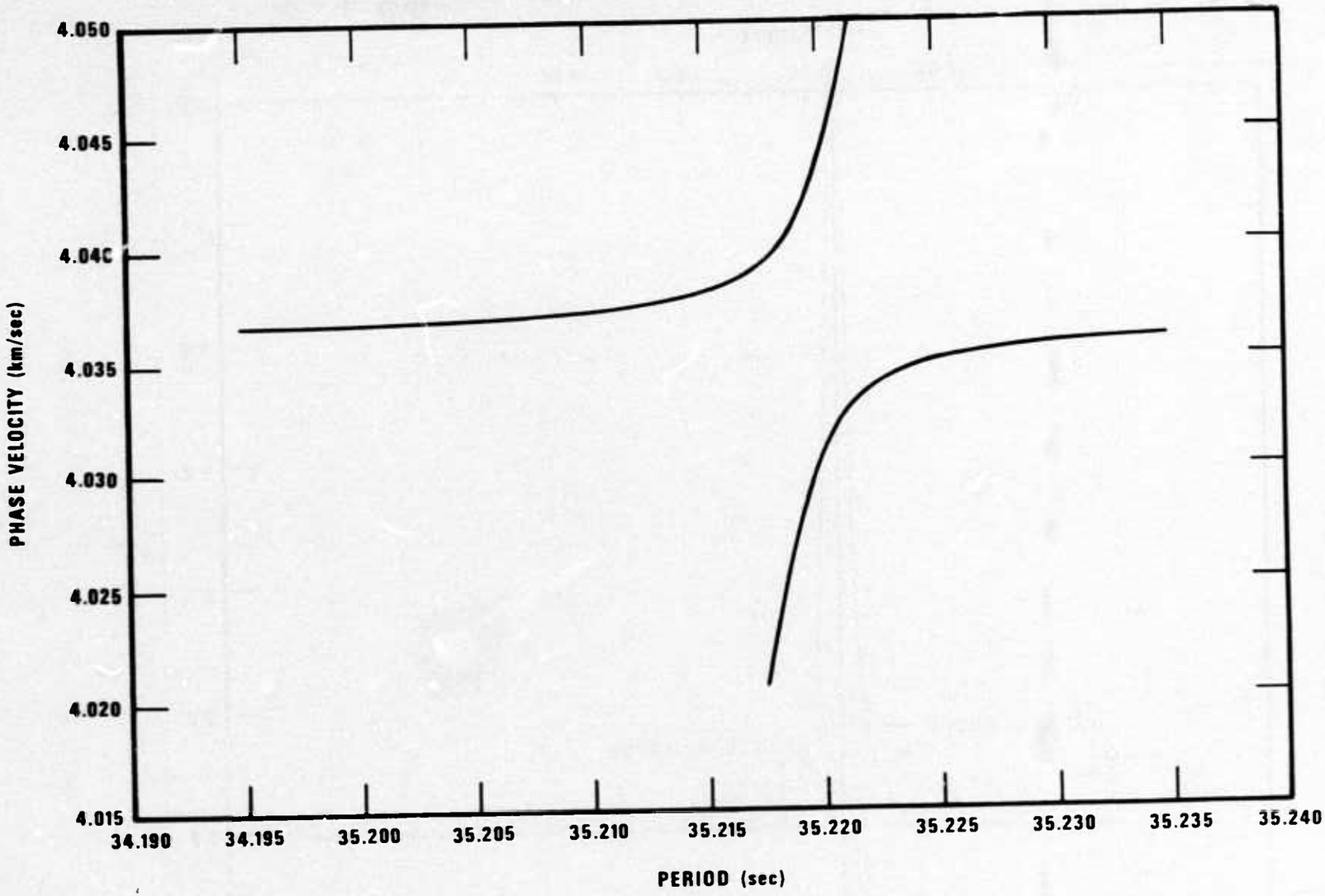

Figure 3. Region of the c-T plane where the fundamental mode Rayleigh roots and the higher-mode acoustic roots intersect.

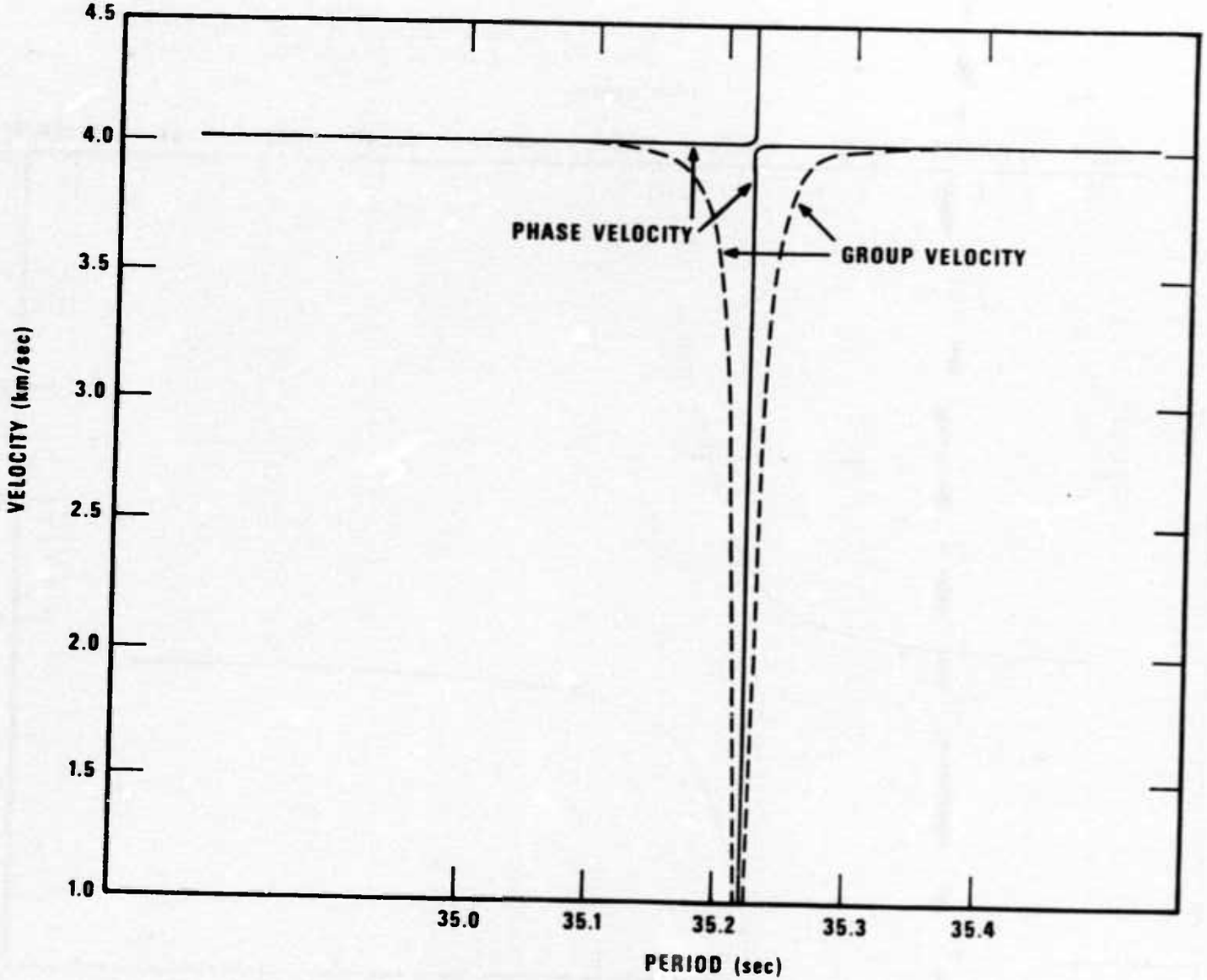

Figure 4. Phase and group velocities for the region shown in Figure 3.

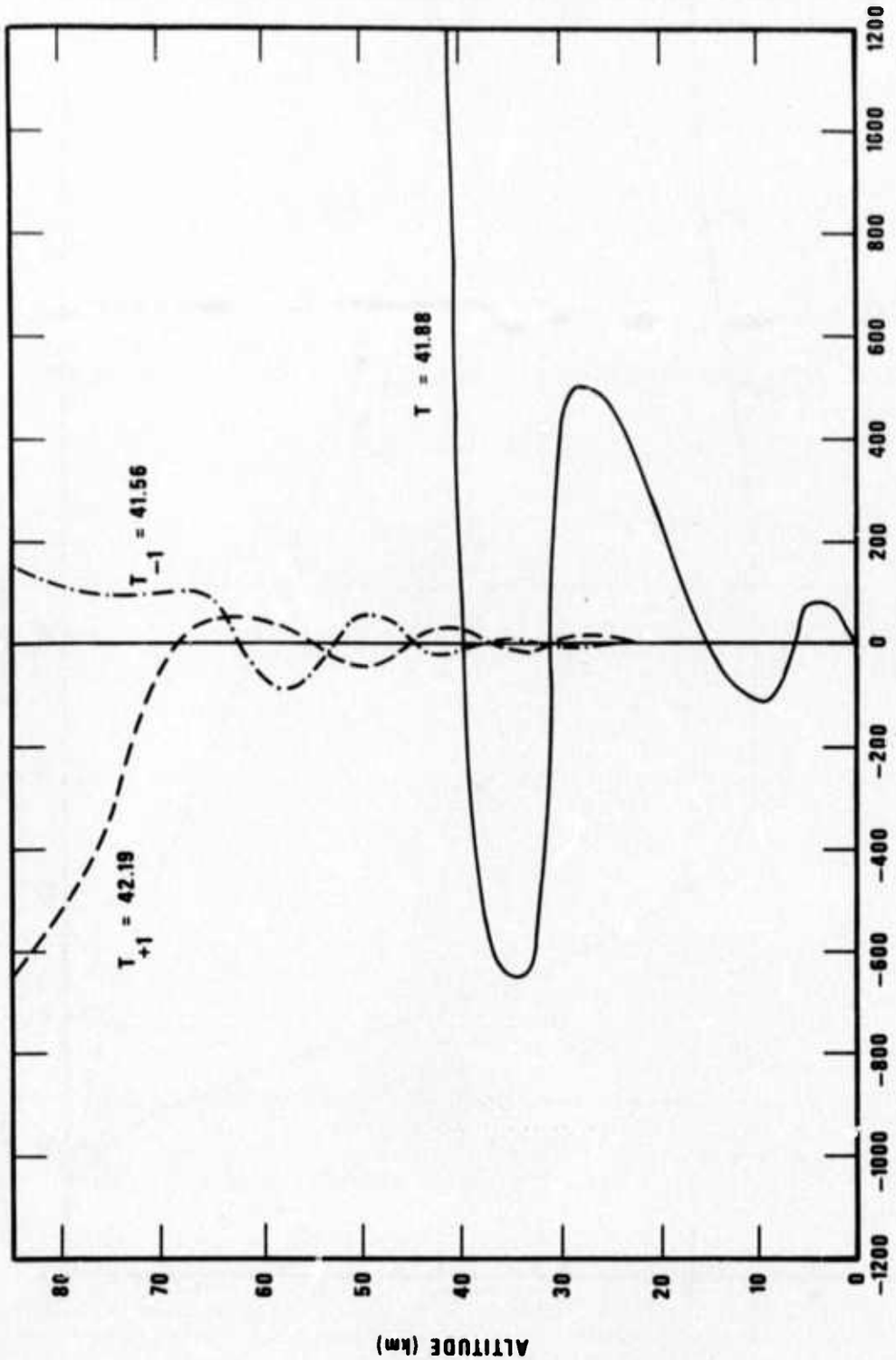

Figure 5. Normalized vertical particle velocity in the atmosphere.

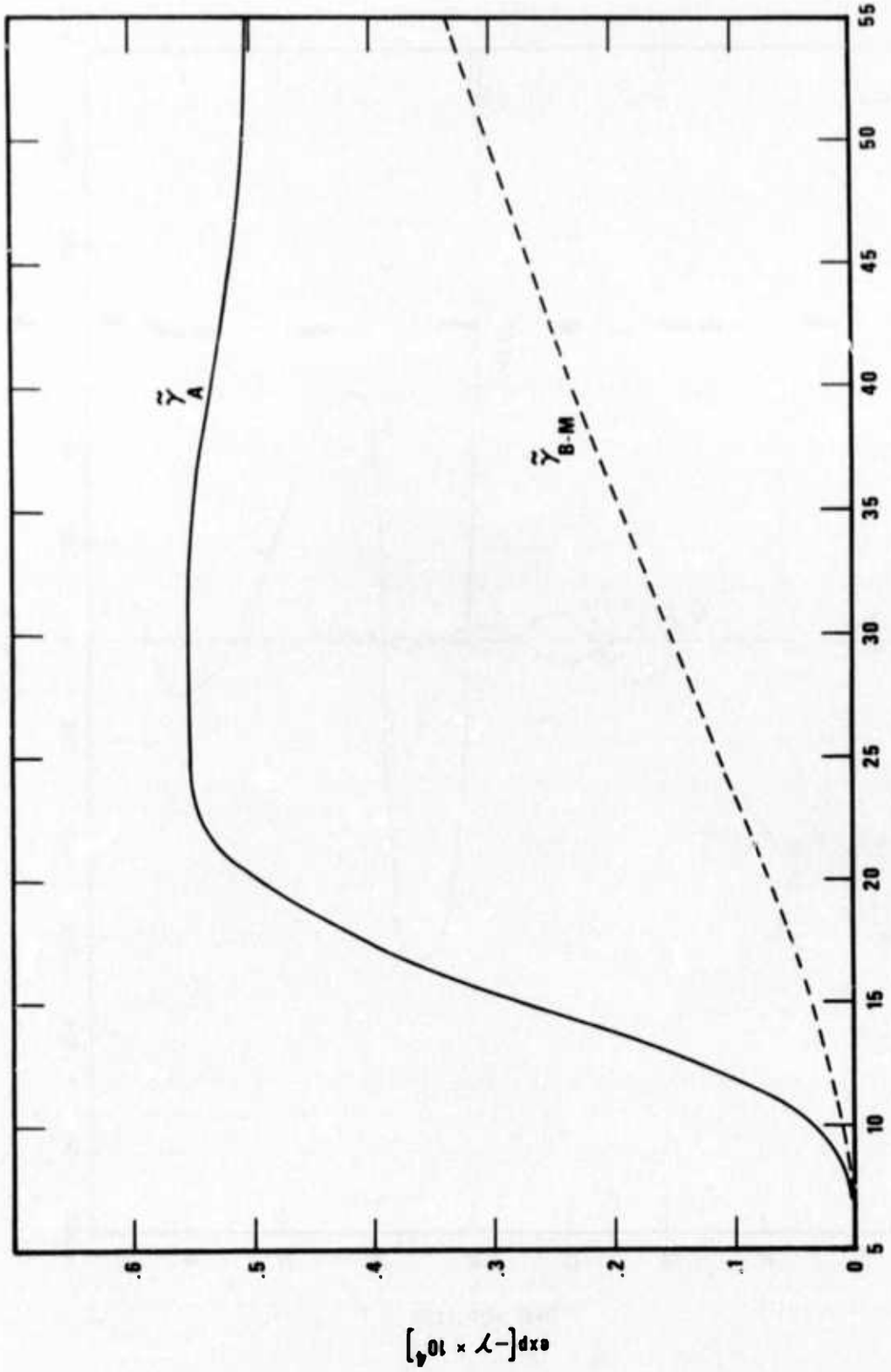

Figure 6. Spectral decay factors $\exp(-\hat{\gamma}_A\Delta)$ and $\exp(-\hat{\gamma}_{B\text{-}M}\Delta)$ for Δ = 10000 km epicentral distance.

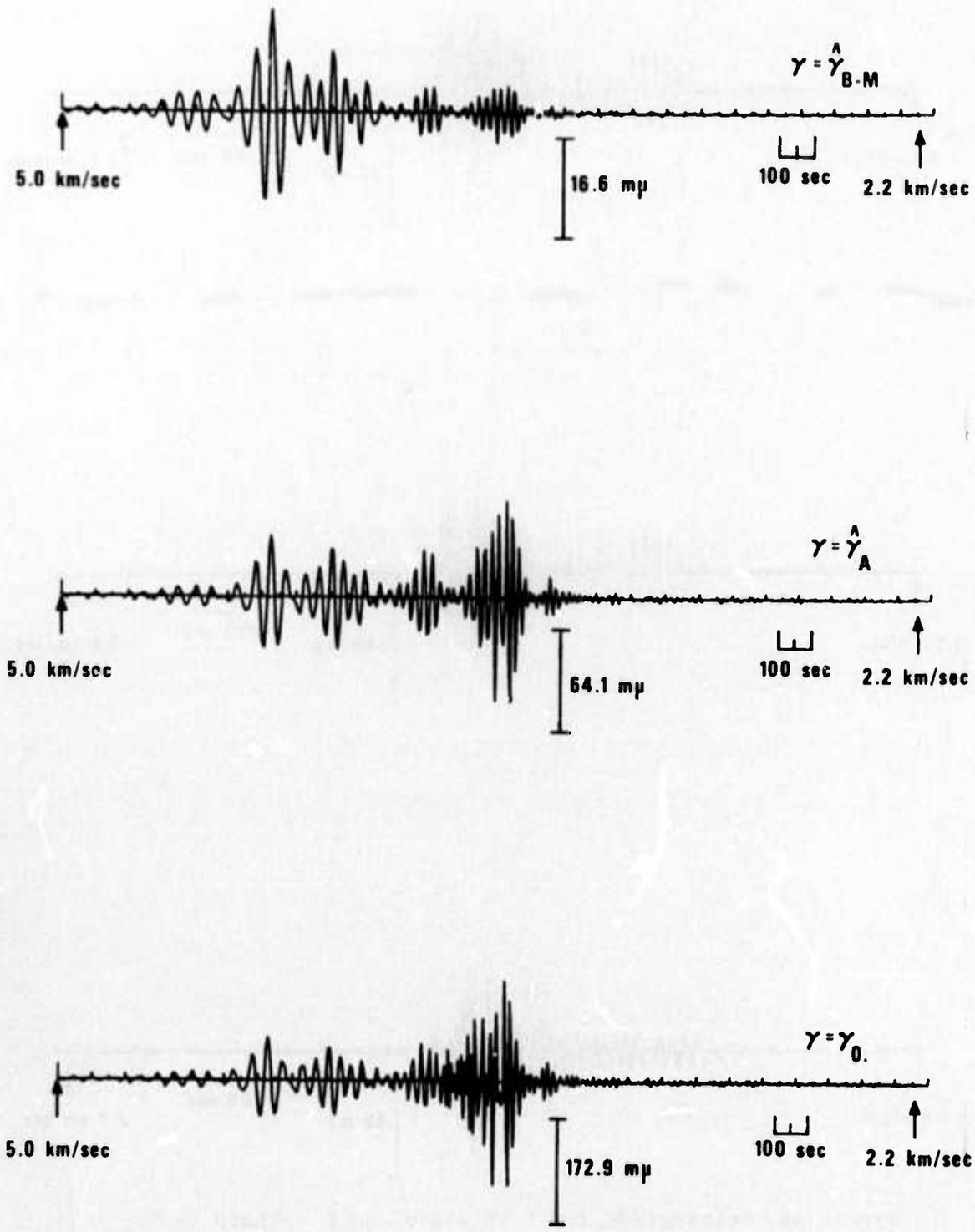

Figure 7. Waveforms for different spectral decay factors described in text. Source altitude is 18.6 km, yield is 100 kT, and epicentral distance is 10000 km.

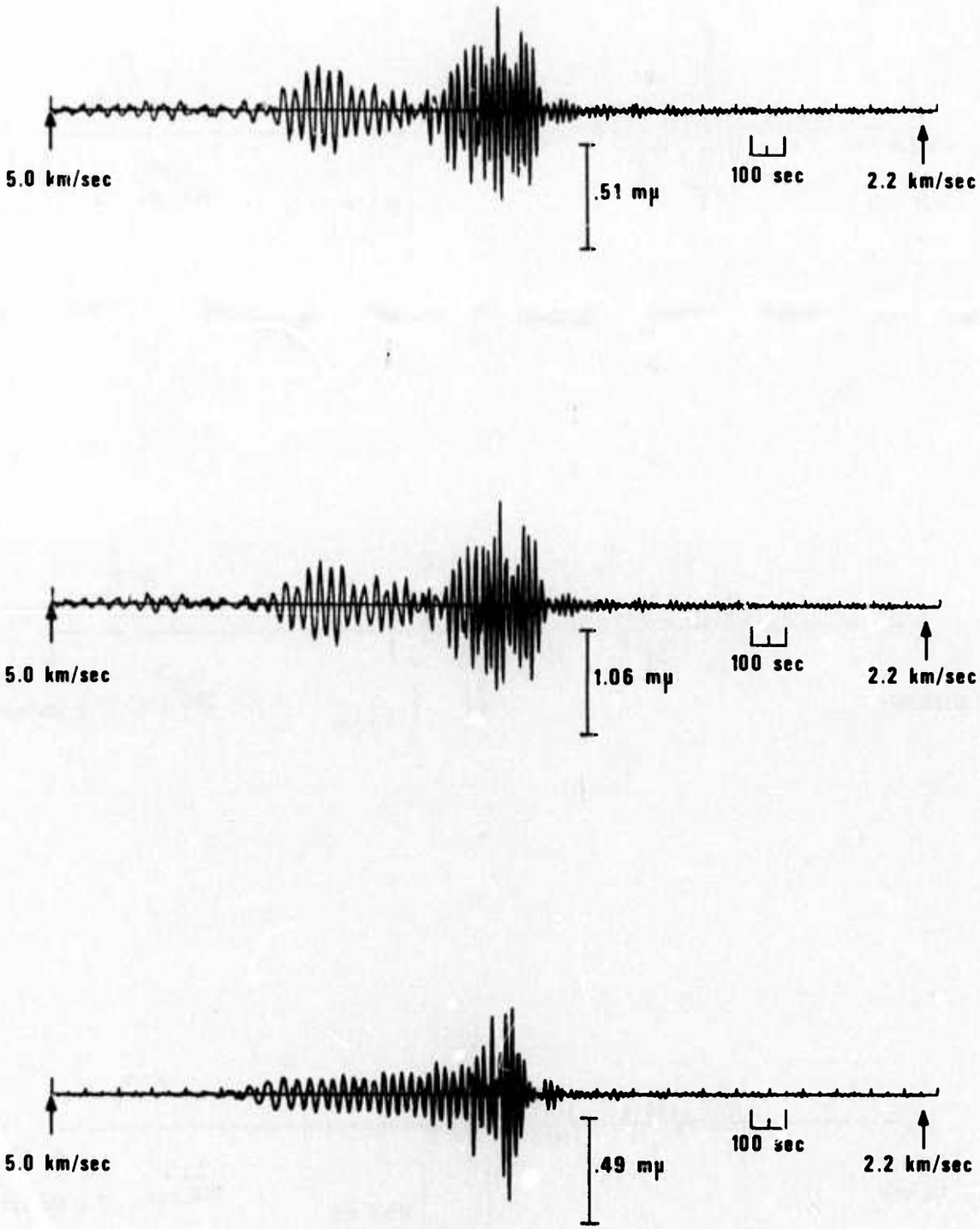

Figure 8a. Seismograms for 1 kT yield and Δ = 10000 km for different source types, source altitudes, and earth models. Continental model, source at 0.305 km. In each case the upper seismogram for a mass-injection source, the middle seismogram for an energy-injection source, and the lower seismogram for a surface overpressure source.

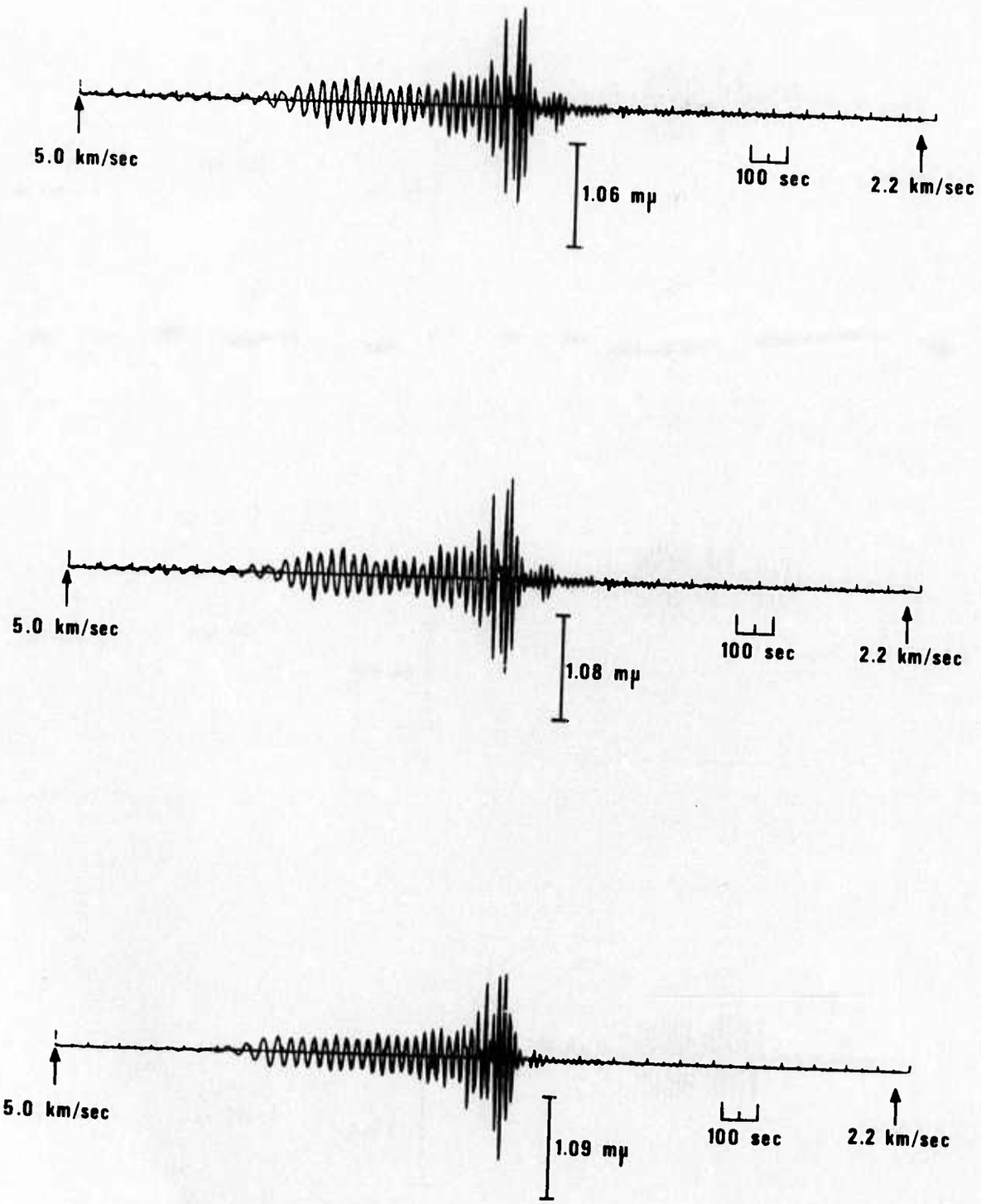

Figure 8b. Seismograms for 1 kT yield and Δ = 10000 km for different source types, source altitudes, and earth models. Continental model, source at 1.83 km. In each case the upper seismogram for a mass-injection source, the middle seismogram for an energy-injection source, and the lower seismogram for a surface overpressure source.

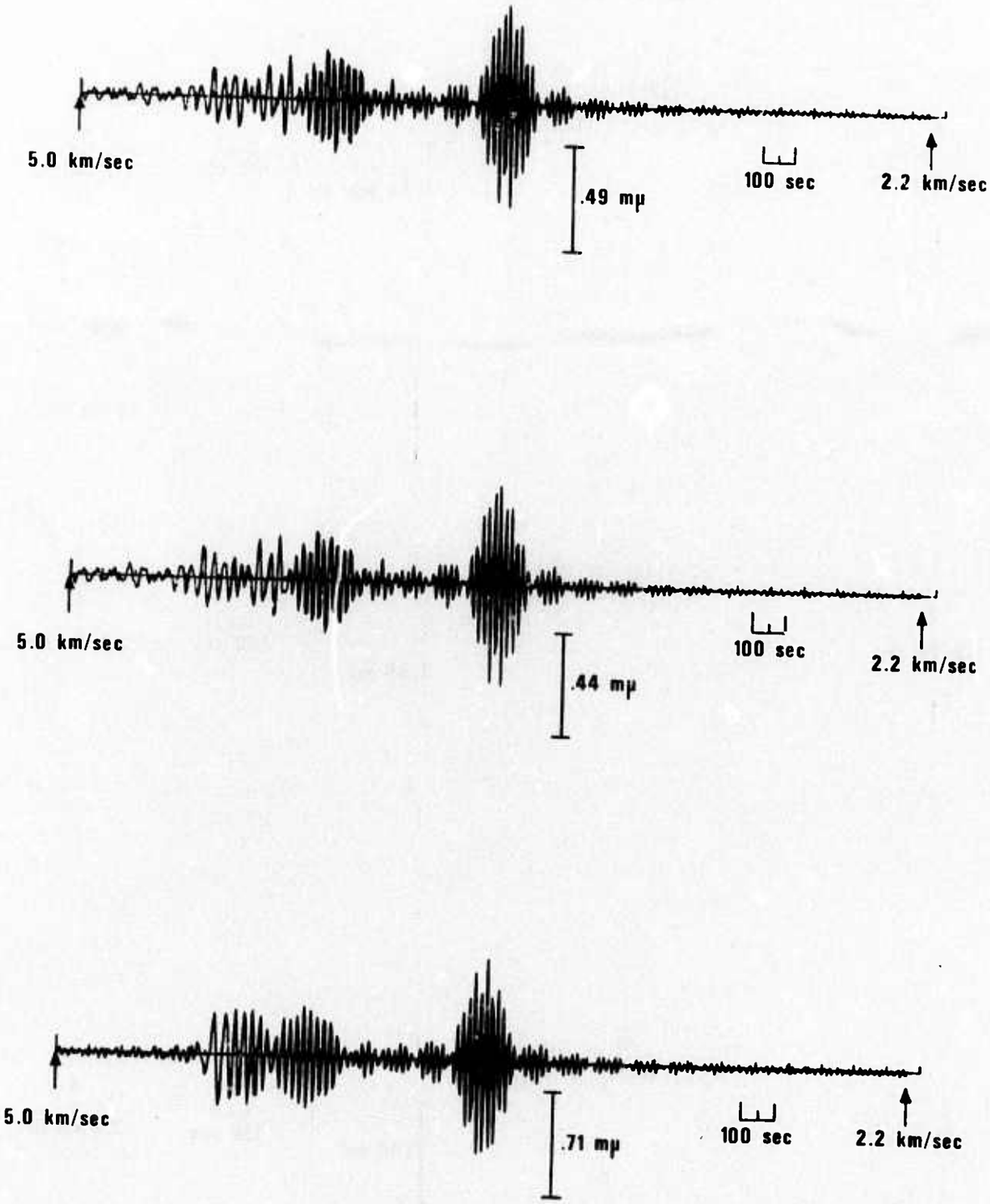

Figure 8c. Seismograms for 1 kT yield and Δ = 10000 km for different source types, source altitudes, and earth models. Oceanic model, source at 0.305 km. In each case the upper seismogram for a mass-injection source, the middle seismogram for an energy-injection source, and the lower seismogram for a surface overpressure source.

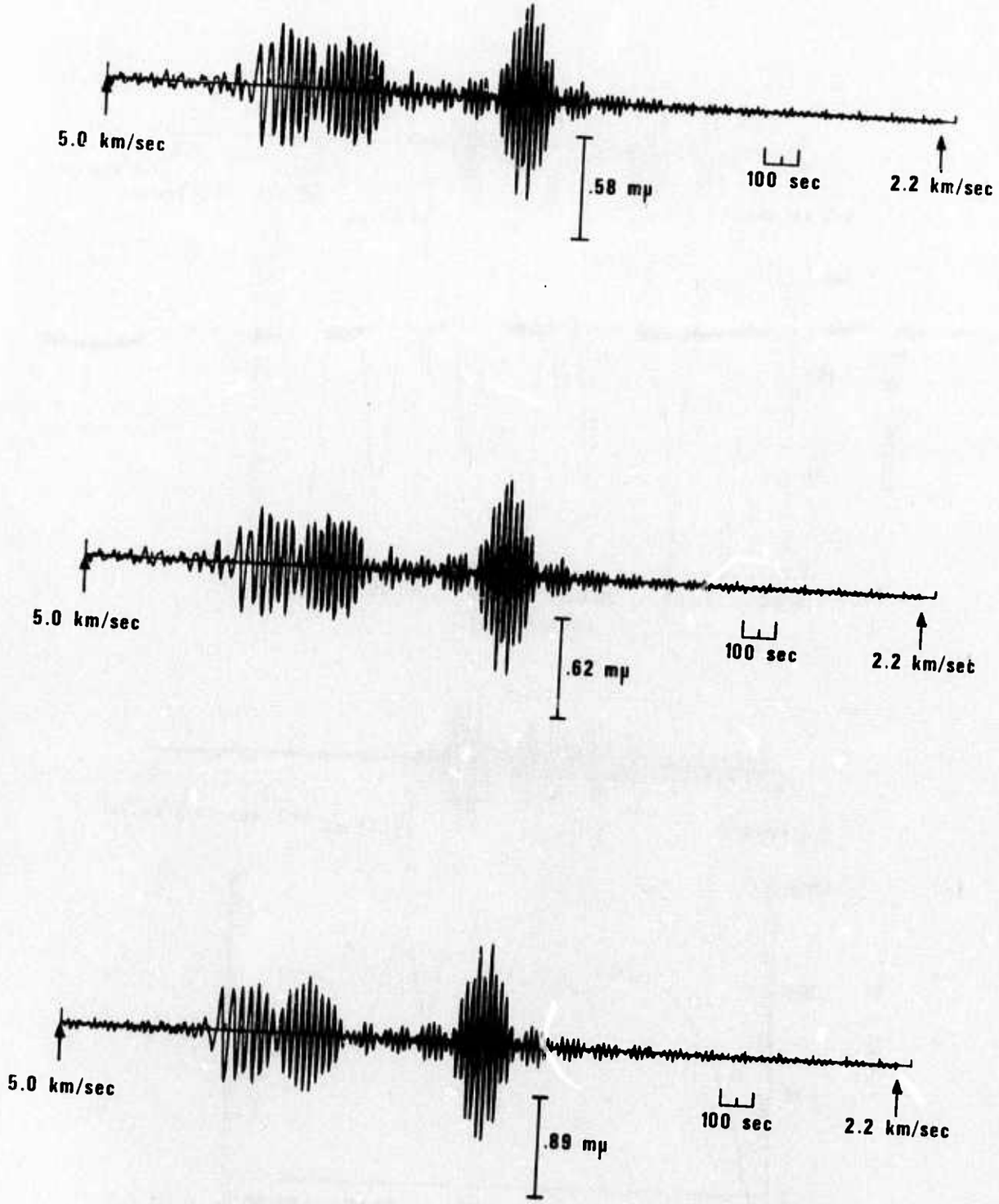

Figure 8d. Seismograms for 1 kT yield and Δ = 10000 km for different source types, source altitudes, and earth models. Oceanic models, source at 1.83 km. In each case the upper seismogram for a mass-injection source, the middle seismogram for an energy-injection source, and the lower seismogram for a surface overpressure source.

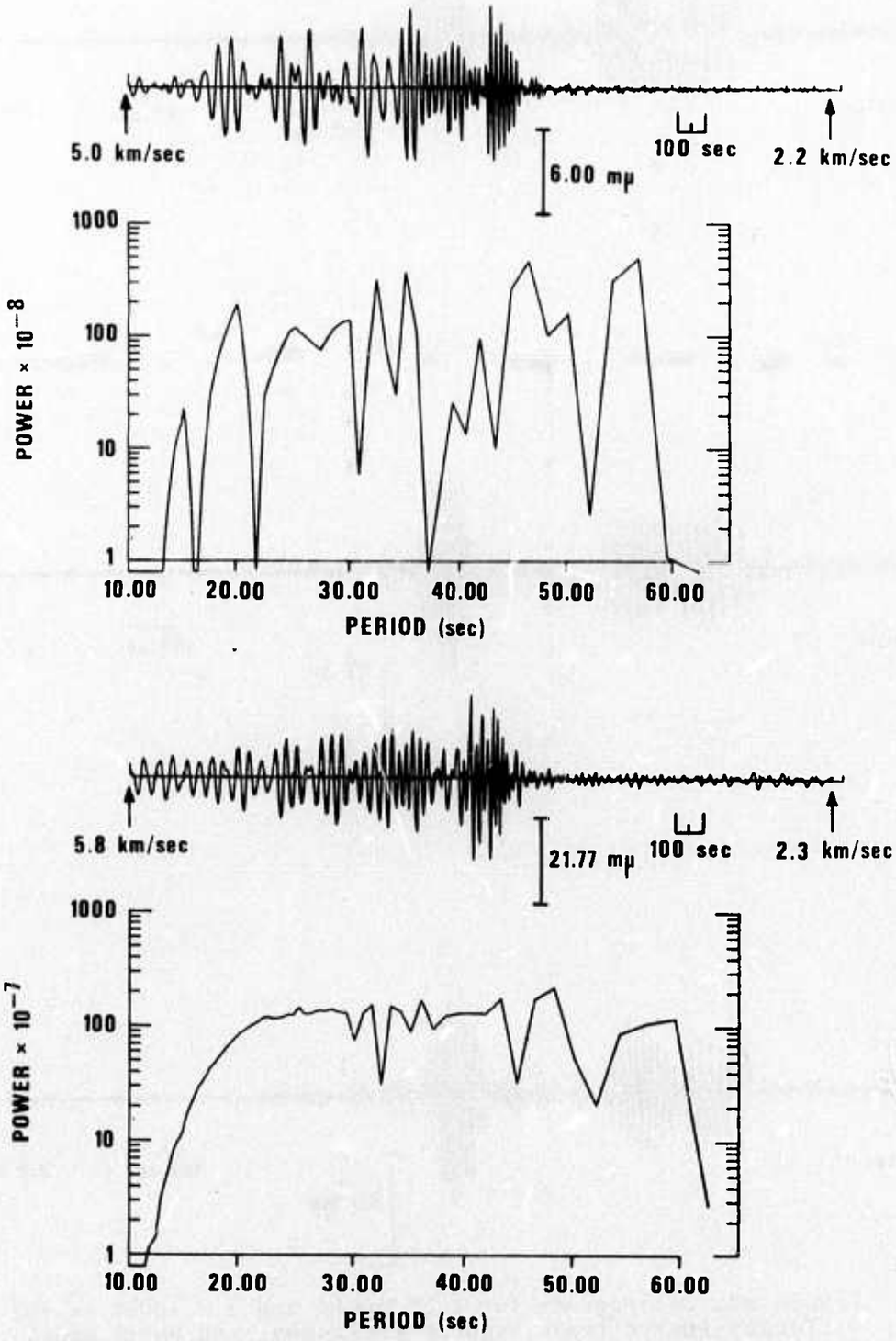

Figure 9a. Seismograms and amplitude spectra for intermediate source altitudes. Continental earth model, for epicentral distance Δ = 10000 km. The upper figures show results for an energy injection source and the lower figures for a surface overpressure source, 10 kT at 82.3 km altitude.

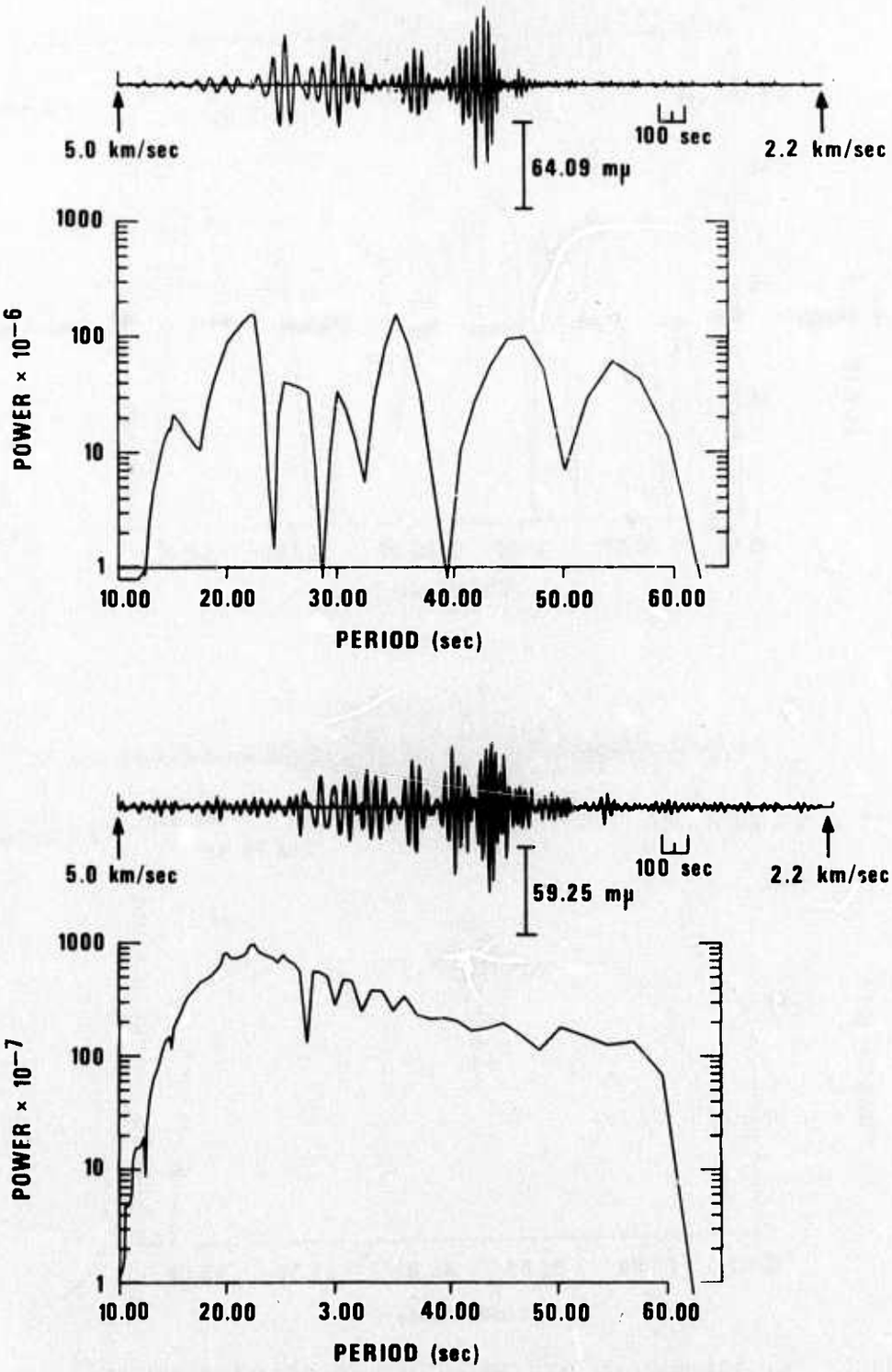

Figure 9b. Seismograms and amplitude spectra for intermediate source altitudes. Continental earth model, for epicentral distance Δ = 10000 km. The upper figures show results for an energy injection source and the lower figures for a surface overpressure source, 100 kT at 18.6 km altitude.

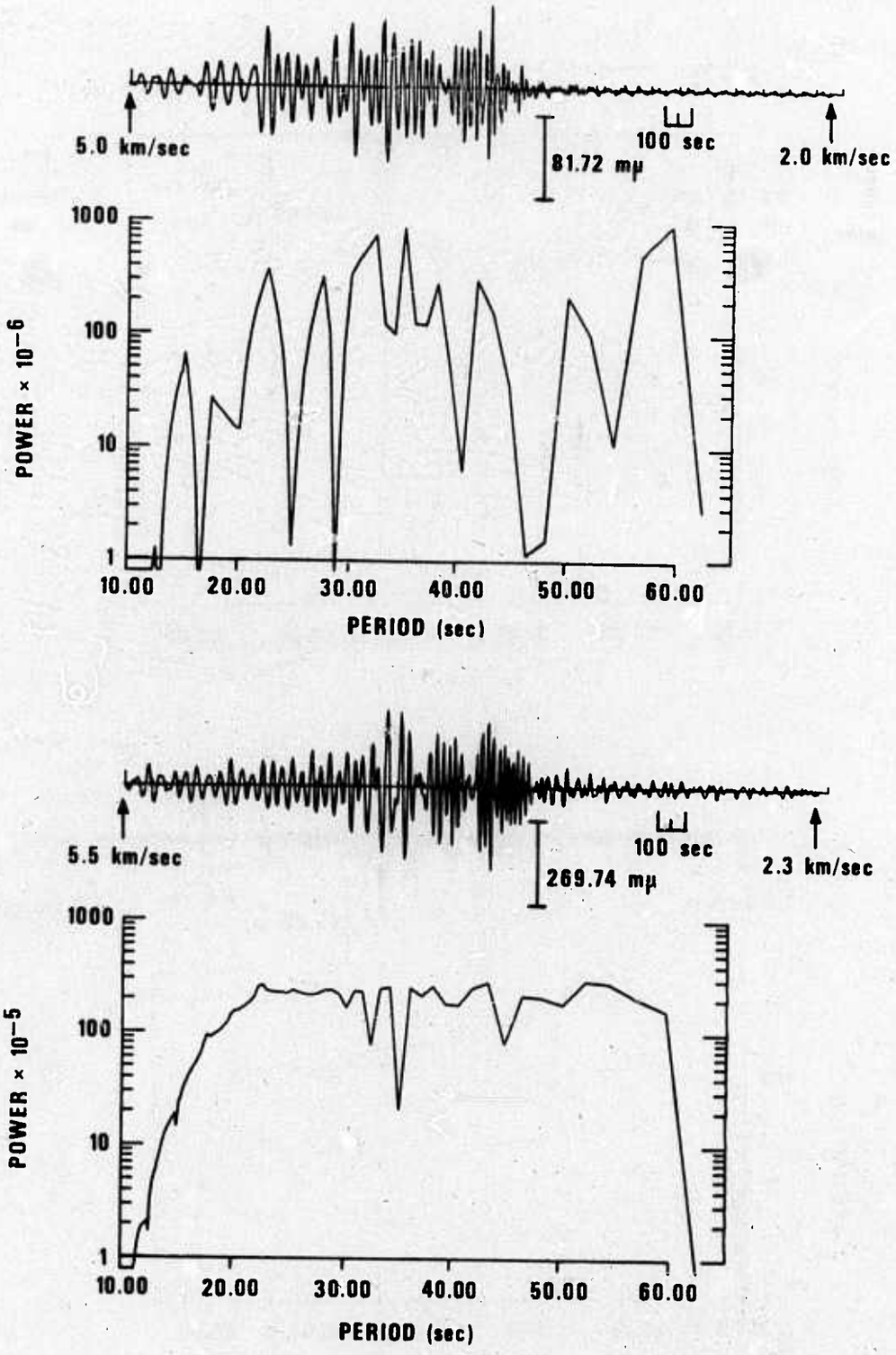

Figure 9c. Seismograms and amplitude spectra for intermediate source altitudes. Continental earth model, for epicentral distance Δ = 10000 km. The upper figures show results for an energy injection source and the lower figures for a surface overpressure source, 1 MT at 51.2 km altitude.

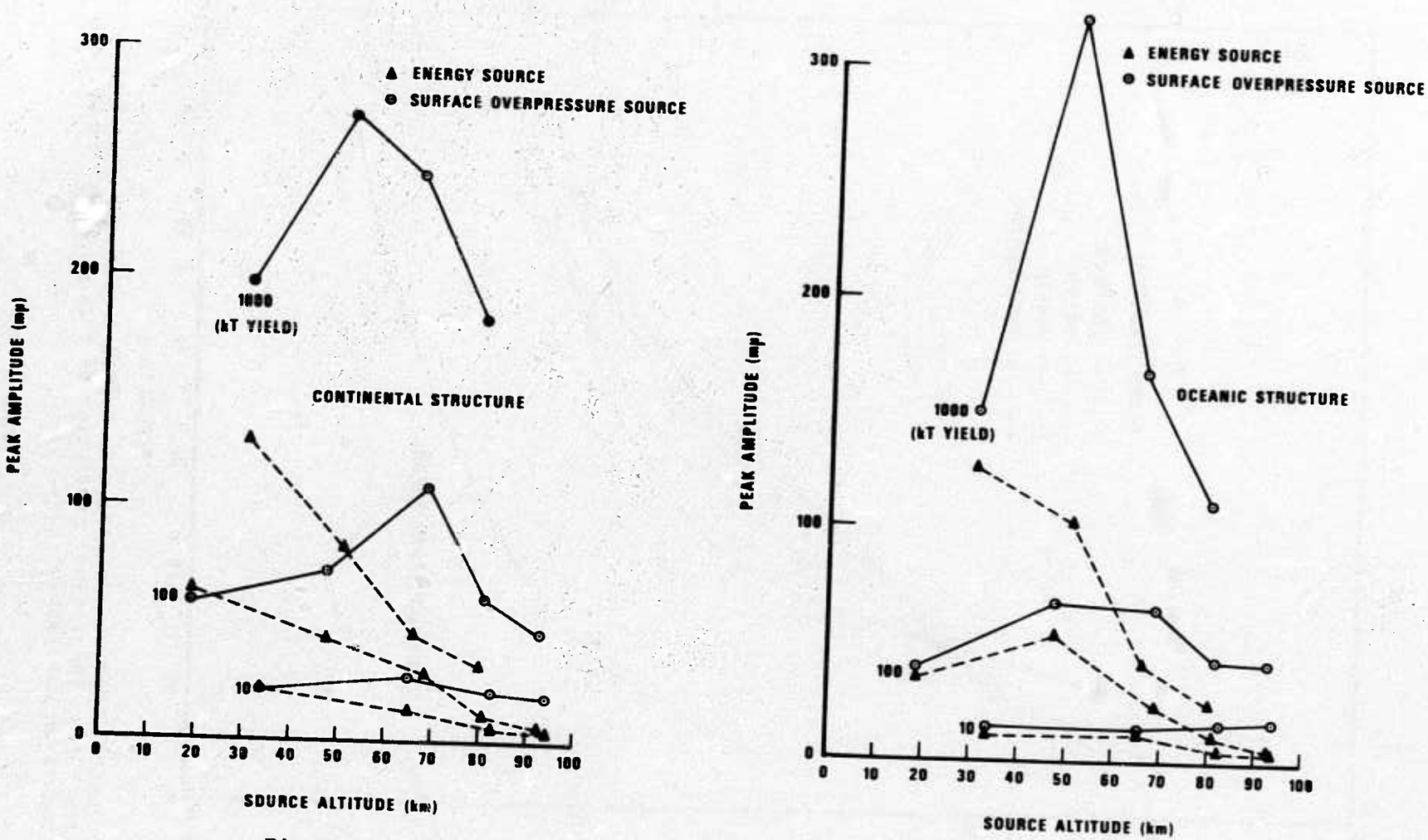

Figure 10. Peak Rayleigh wave amplitude for intermediate source altitudes, for energy injection and surface overpressure sources.

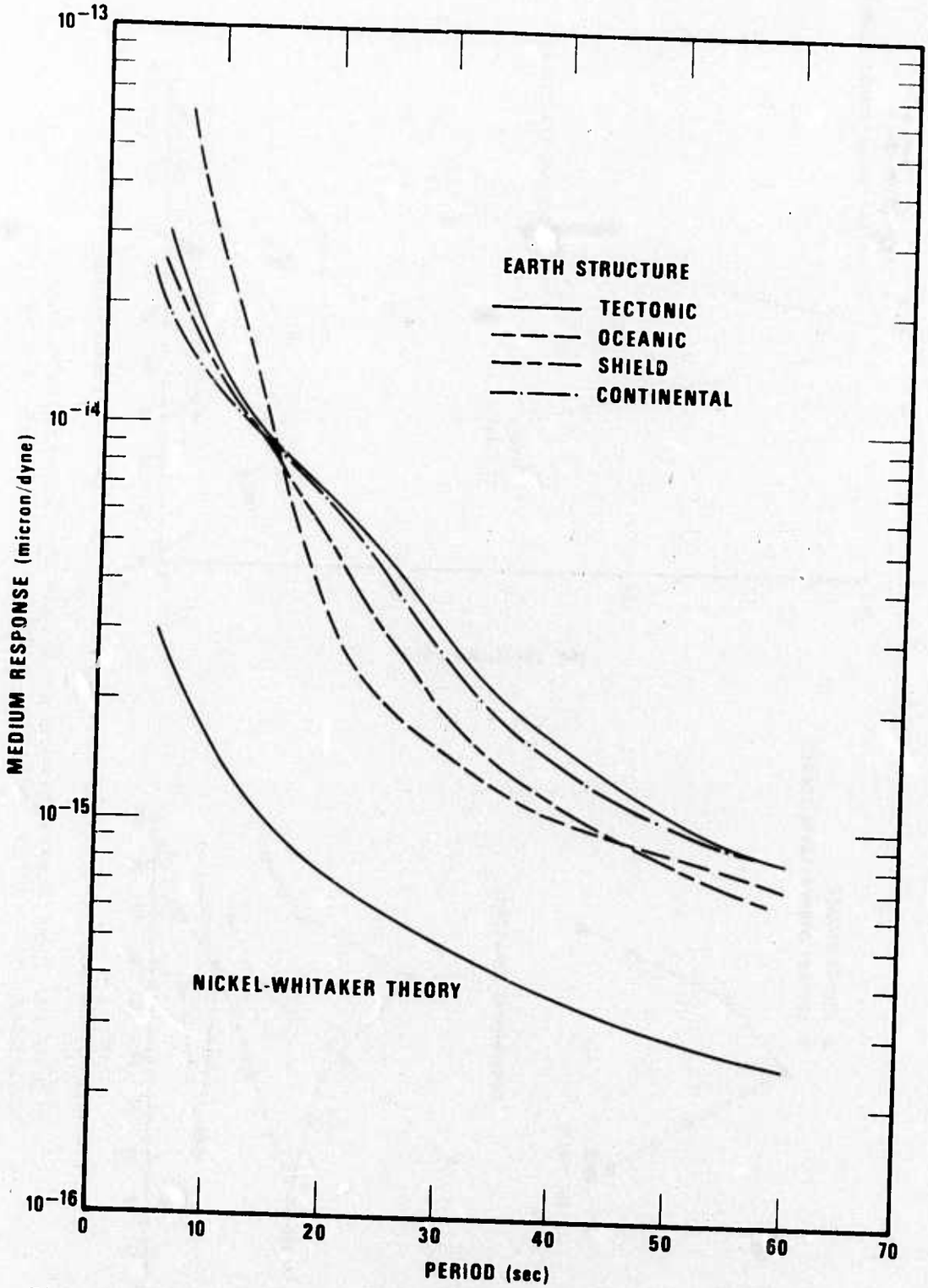

Figure 11. Medium response as a function of period for four earth structures. Theoretical prediction of Nickel and Whitaker shown for comparison and labeled $\rho\Lambda_R$.

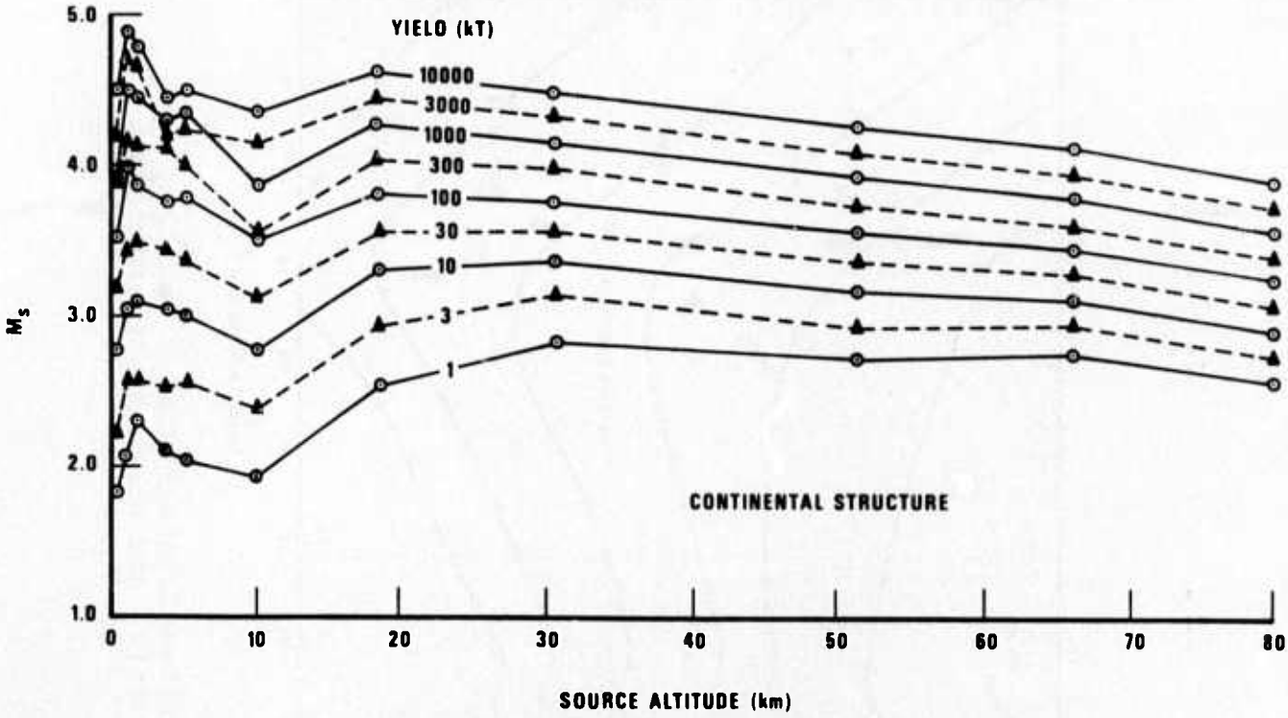

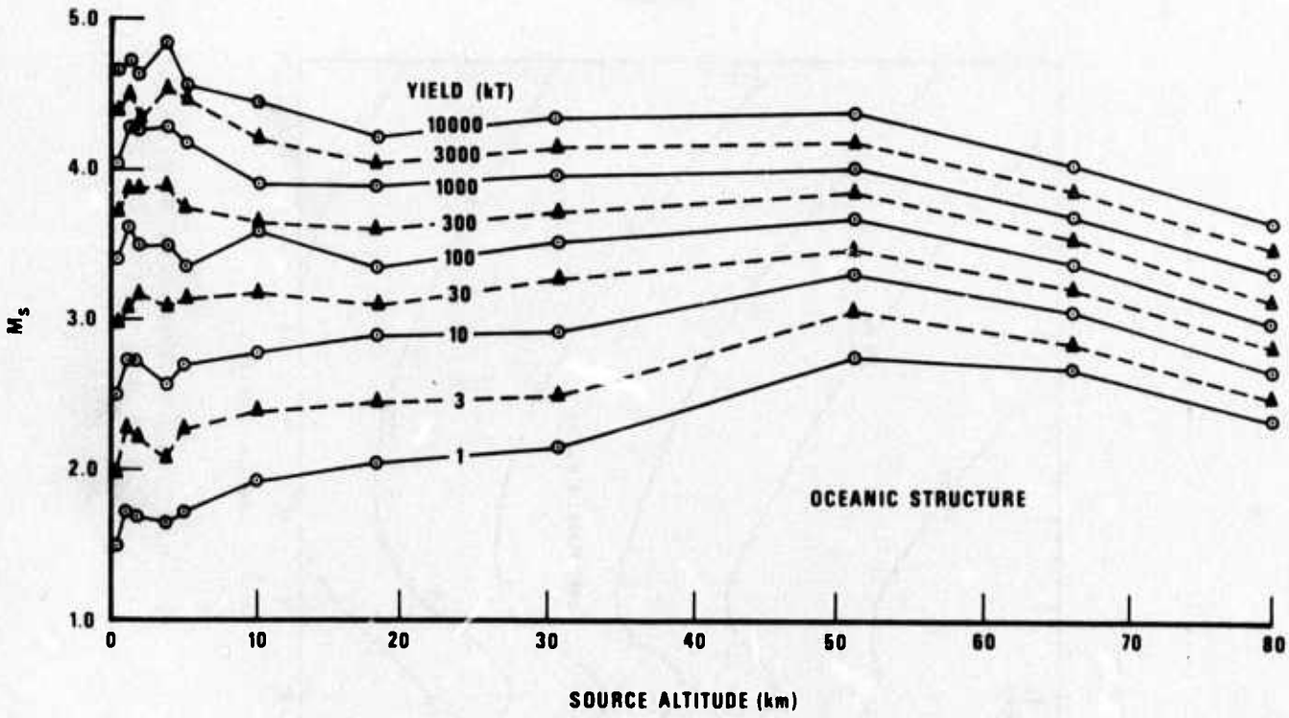

Figure 12. M_S as a function of source altitude with yield as a parameter, for continental and oceanic structures.

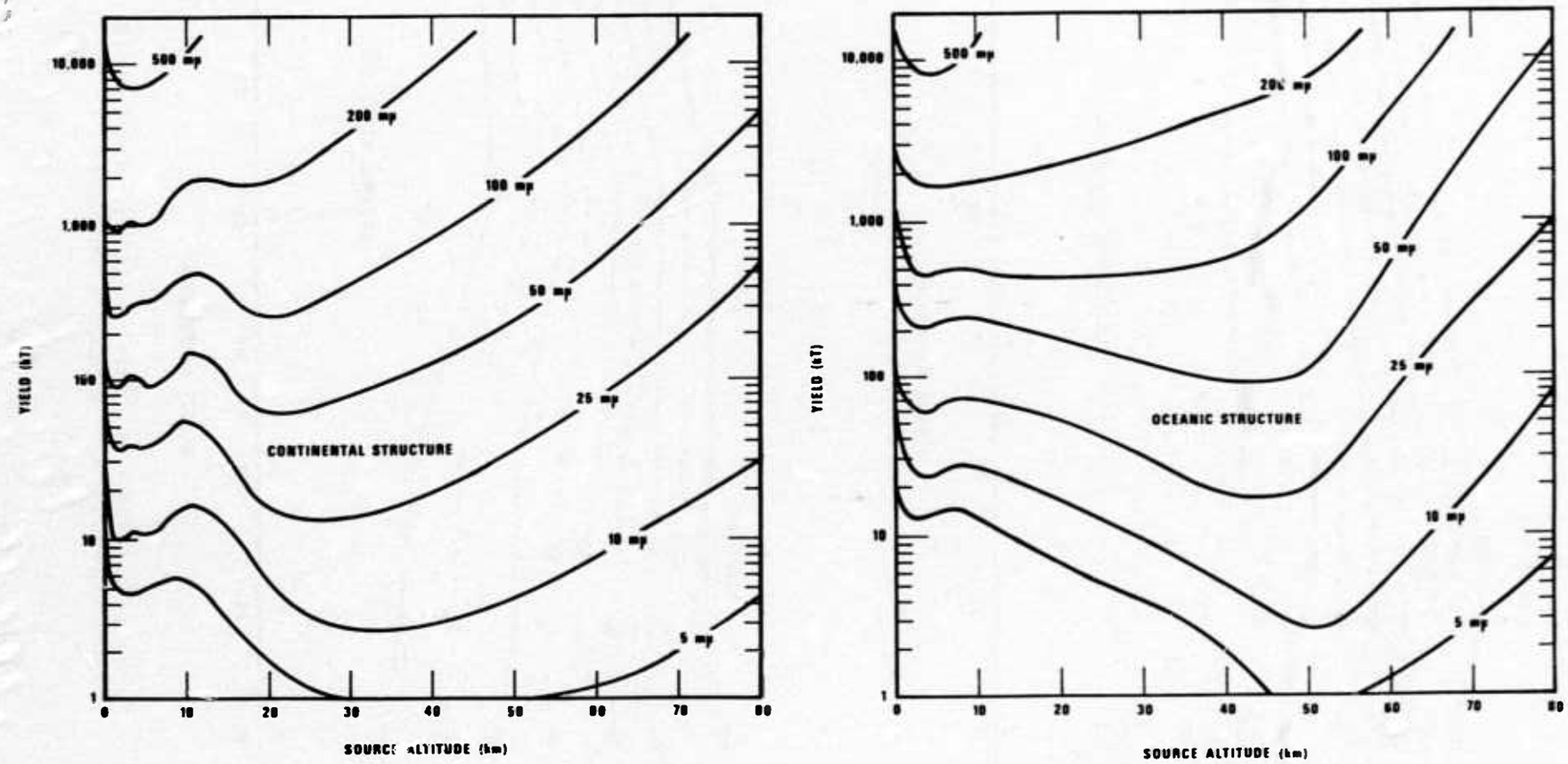

Figure 13. Maximum Rayleigh wave amplitude contoured as a function of yield and burst height, for continental and oceanic structure.

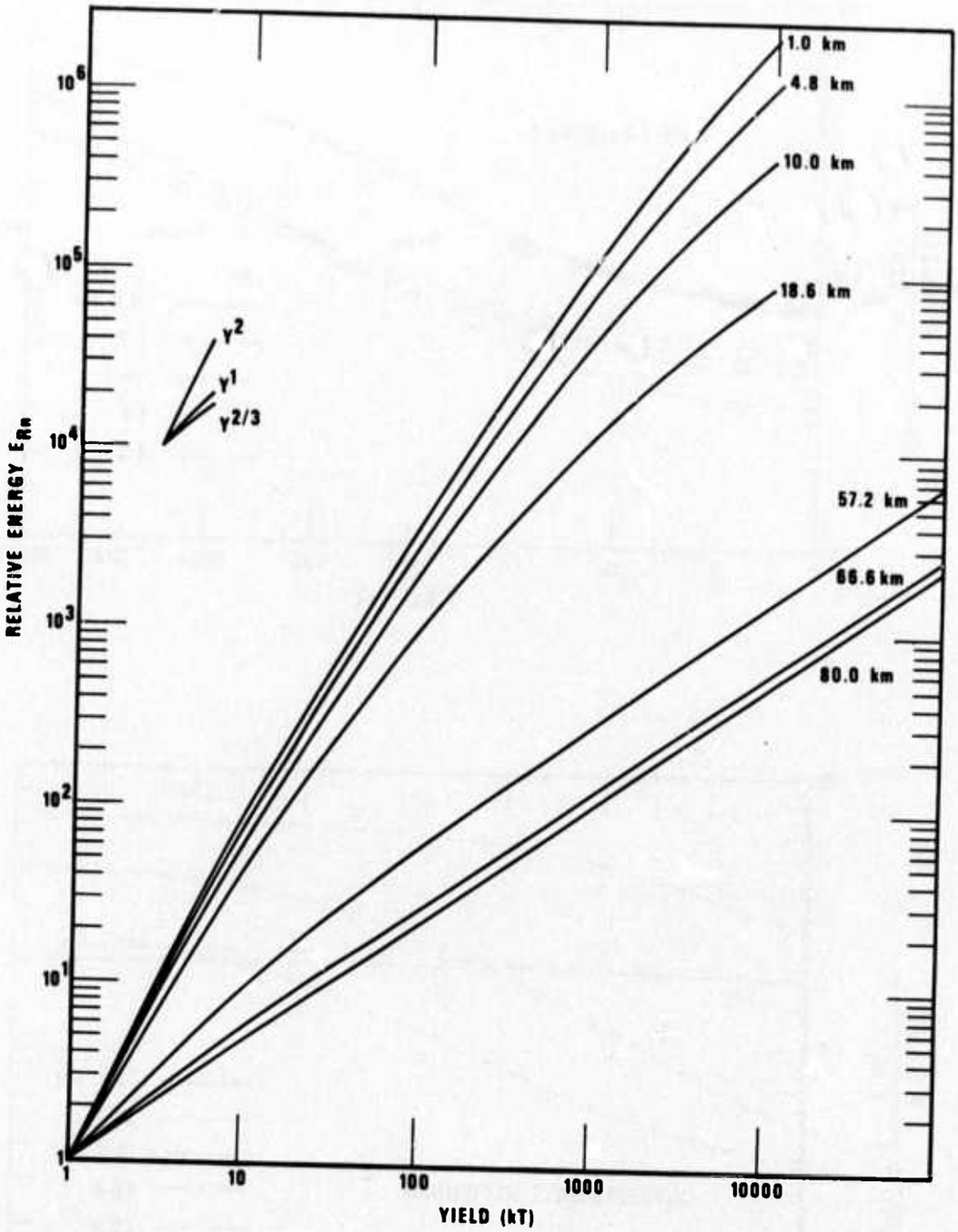

Figure 14. Spectral energy (normalized at 20 seconds period) as a function of yield. Sources at altitudes 1.0 to 80.0 km over a continental earth model. Reference lines show W^2, W^1, and $W^{2/3}$ yield dependence.

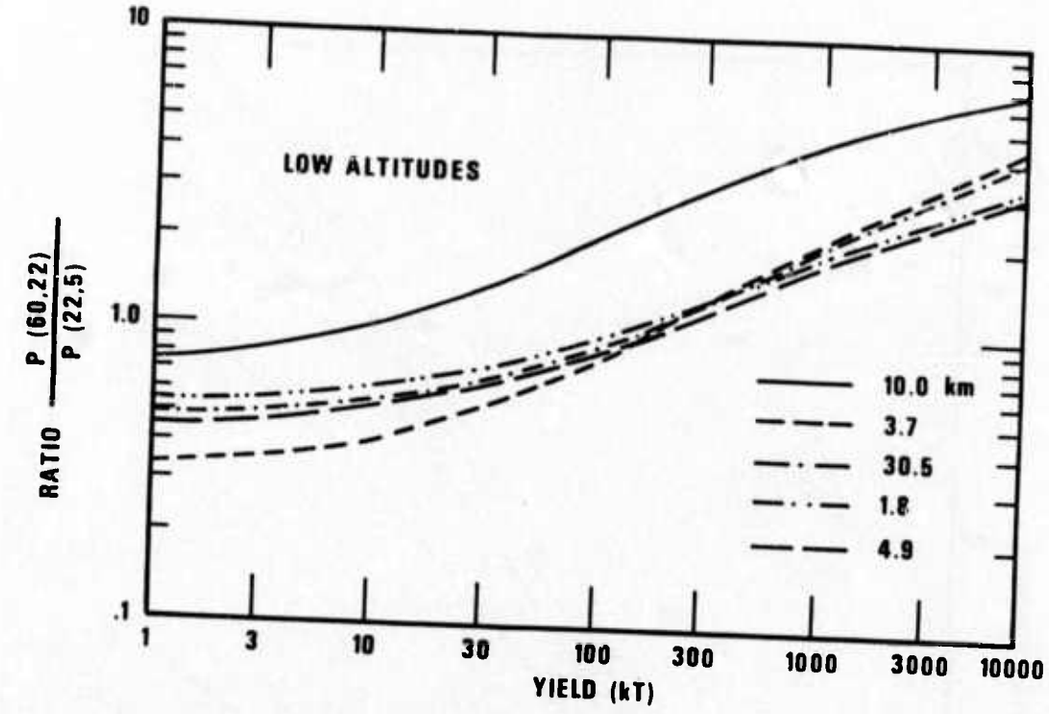

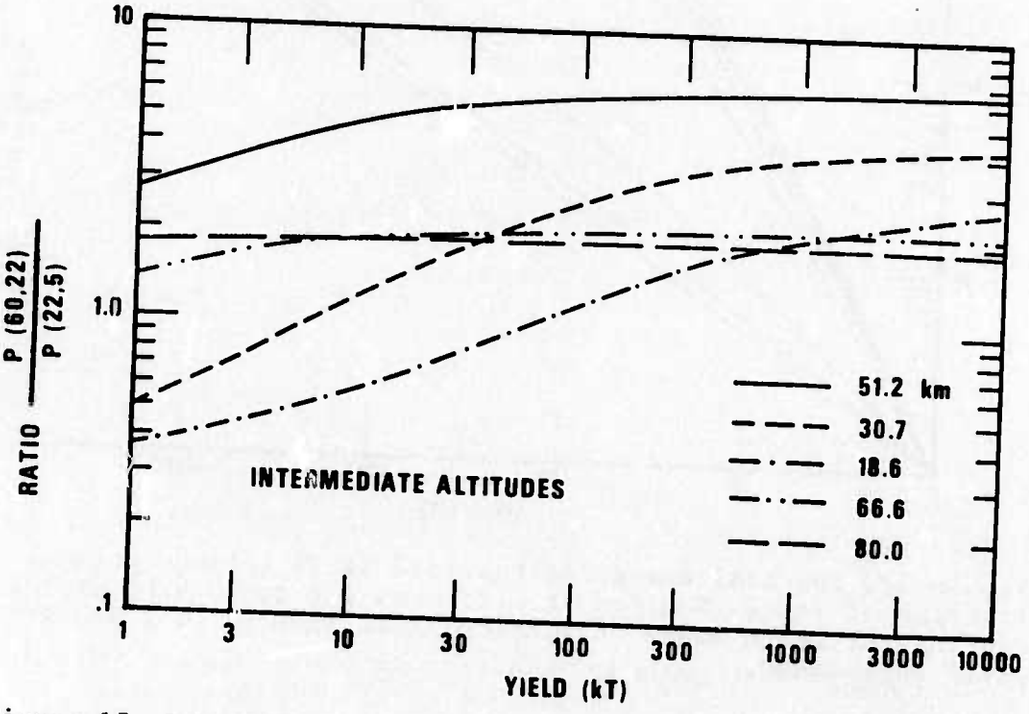

Figure 15. Spectral power ratio $\langle R \rangle_{22}$ as a function of yield, for continental earth structure. Upper figure for low source altitudes, lower for intermediate altitudes.

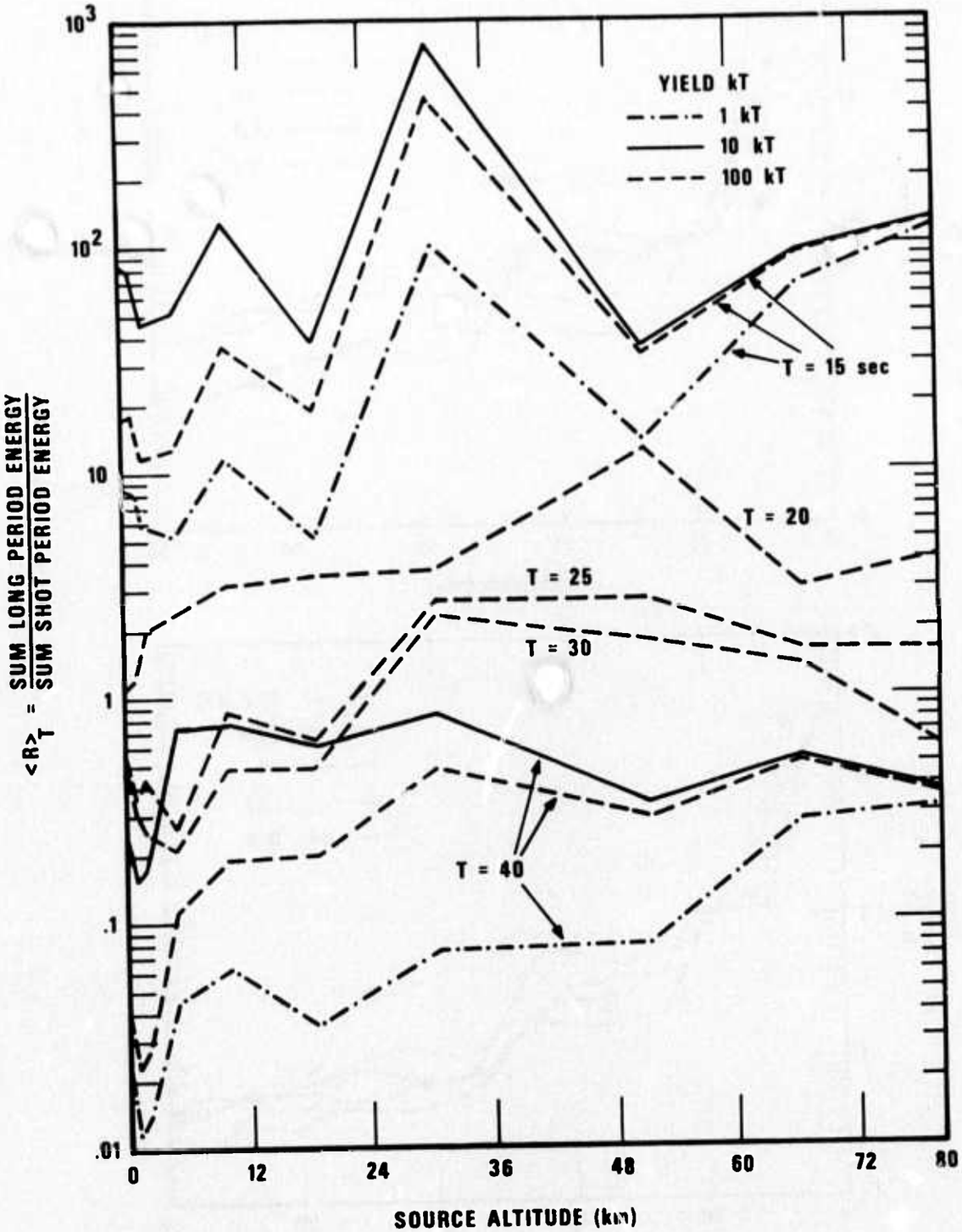

Figure 16. Spectral power ratio <R>22 as a function of source altitude, for T = 15 to 40 seconds, and for three source yields. Continental earth model.

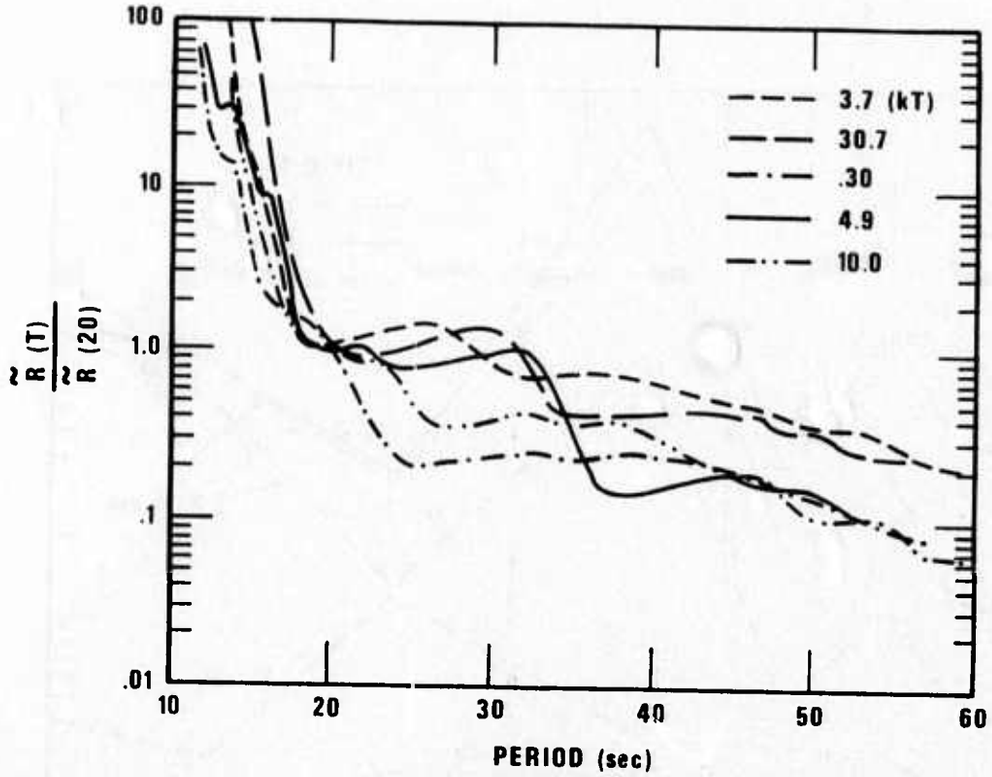

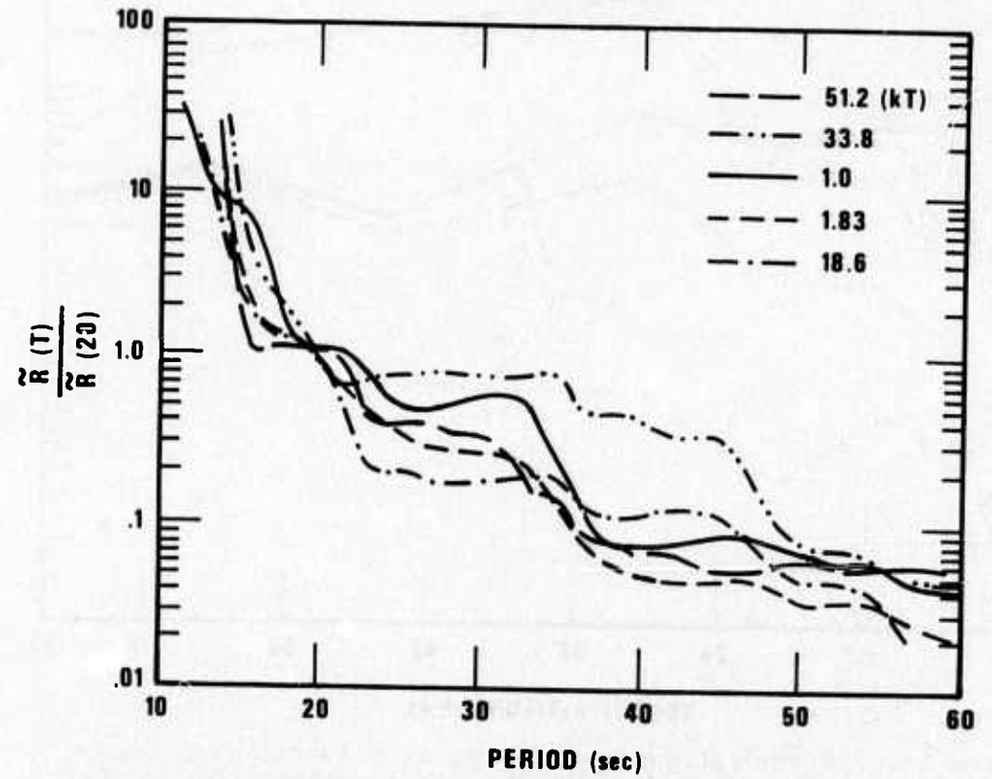

Figure 17. $\tilde{R}(T)$ normalized at T = 20 seconds period, for different source altitudes. The data are separated into two groups simply for clarity of presentation.

TABLE 1

Calculated fundamental mode Rayleigh wave velocities, surface ellipticity, and medium responses for atmosphere continental and atmosphere oceanic models

Period T (sec)	Absorption coefficient γ_A (10^{-4}km^{-1})	Phase velocity c (km/sec)	Group velocity U (km/sec)	Ellipticity u_o/w_o	Medium response A_e (10^{-11} microns/dyne)	Phase velocity c (km/sec)	Group velocity U (km/sec)	Ellipticity u_o/w_o	Medium response A_e (10^{-11} microns/dyne)
60.0	0.695	3.9692	3.8589	-0.846	8.0907E-5	4.0366	4.0214	-0.743	7.3237E-5
57.5	0.690	3.9645	3.8543	-0.844	8.5144E-5	4.0362	4.0260	-0.747	7.6003E-5
55.0	0.686	3.9596	3.8479	-0.840	9.0004E-5	4.0360	4.0303	-0.751	7.9053E-5
52.5	0.680	3.9542	3.8401	-0.836	9.5646E-5	4.0359	4.0354	-0.755	8.2442E-5
50.0	0.675	3.9484	3.8265	-0.830	1.0227E-4	4.0360	4.0368	-0.760	8.6237E-5
47.5	0.665	3.9419	3.8089	-0.823	1.1013E-4	4.0364	4.0382	-0.764	9.0505E-5
45.0	0.655	3.9343	3.7884	-0.815	1.1967E-4	4.0367	4.0396	-0.769	9.4505E-5
42.5	0.643	3.9252	3.7607	-0.805	1.3137E-4	4.0370	4.0395	-0.774	1.0105E-4
40.0	0.630	3.9141	3.7231	-0.793	1.4604E-4	4.0372	4.0354	-0.779	1.0768E-4
37.5	0.608	3.9001	3.6722	-0.780	1.6479E-4	4.0370	4.0245	-0.784	1.1558E-4
35.0	0.600	3.8821	3.6067	-0.764	1.8925E-4	4.0362	4.0118	-0.789	1.2516E-4
32.5	0.590	3.8584	3.5235	-0.747	2.2186E-4	4.0344	3.9917	-0.794	1.3798E-4
30.0	0.590	3.8267	3.4300	-0.729	2.6605E-4	4.0306	3.9674	-0.798	1.5230E-4
27.5	0.590	3.7844	3.3107	-0.711	3.2598E-4	4.0242	3.9258	-0.801	1.7230E-4
25.0	0.595	3.7285	3.1826	-0.694	4.0564E-4	4.0131	3.8694	-0.802	1.9971E-4
22.5	0.610	3.6576	3.0822	-0.680	5.0559E-4	3.9942	3.7748	-0.797	2.3978E-4

Table 1 Cont'd.

Period T (sec)	Absorption coefficient $\hat{\gamma}_A$ (10^{-4} km^{-1})	Phase velocity c (km/sec)	Group velocity U (km/sec)	Ellip-ticity u_o/w_o	Medium response A (10^{-11} microns/dyne)	Phase velocity c (km/sec)	Group velocity U (km/sec)	Ellip-ticity u_o/w_o	Medium response A (10^{-11} microns/dyne)
20.0	0.700	3.5740	2.9777	-0.672	6.1978E-4				
18.75	0.775					3.9323	3.4619	-0.761	3.5715E-4
17.5	0.900	3.4857	2.9511	-0.669	7.3836E-4	3.8898	3.2399	-0.728	4.3746E-4
16.0	1.0875					3.7964	2.7132	-0.653	6.2266E-4
15.0	1.250	3.4027	2.9817	-0.671	8.5923E-4				
14.375	1.400					3.5264	1.5386	-0.472	1.1956E-3
13.500	1.600					3.1781	1.0012	-0.323	1.7682E-3
12.5	2.00	3.338	3.0510	-0.675	9.9608E-4	2.6820	0.8380	-0.186	2.1067E-3
10.675	2.920					2.0764	0.9491	-0.054	2.4357E-3
10.5	3.00	3.2919	3.1049	-0.679	1.1370E-3				
9.0	4.150	3.2687	3.1442	-0.682	1.2801E-3				
7.5	5.500					1.6473	1.1008	+0.090	4.4731E-3
5	9.950					1.4700	1.1837		1.5078E-2
4.0	13.250	3.2395	3.2061	-0.686	2.6285				

TABLE 2

Peak amplitude corrections for

different attenuation factors

Attenuation coefficient	T_m (sec)	Synthesized Waveform Peak Amplitude	Amplitudes calculated from $\hat{\gamma}_A$ waveform
$\hat{\gamma}_o = o$	21	173	123
	46	74	75
$\hat{\gamma}_A$	21	64	
	46	39	
$\hat{\gamma}_{B-M}$	21	5	5
	46	17	18

TABLE 3

Peak Rayleigh wave amplitudes (mμ) for

1 kT yield at low altitudes

	Continental Structure			Oceanic Structure		
Source height (km)	Mass source	Energy source	Surface Overpressure source	Mass source	Energy source	Surface Overpressure source
0.31	0.51	0.49	1.06	0.49	0.44	0.71
1.83	1.06	1.08	1.09	0.58	0.62	0.69
3.66	1.04	0.97	0.99	0.88	0.86	0.71
4.88	1.03	1.08	1.05	0.45	0.52	0.72

TABLE IV

Amplitude, period, and M_s as a function of yield, burst height, and earth model.

		Continental Model				Oceanic Model			
Altitude (km)	Yield	Amplitude (mμ)	Period (sec)	M_s	% Coupling	Amplitude	Period	M_s	% Coupling
.3048	1	.49	17.4	1.82	.000032	.24	18.7	1.47	.000007
.3048	3	1.21	17.4	2.21	.000900	.74	18.7		.000021
.3048	10	4.45	17.4	2.77	.000207	2.55	18.7	2.50	.000005
.3048	30	11.49	17.4	3.18	.000387	7.51	18.7	2.97	.000158
.3048	100	24.79	17.7	3.51	.000442	20.61	18.7	3.41	.000201
.3048	300	55.68	17.7	3.86	.000606	43.96	19.0	3.73	.000366
.3048	1000	111.88	33.2	3.89	.000203	91.66	19.0	4.05	.000378
.3048	3000	221.18	33.2	4.19	.000217	203.37	19.0	4.40	.000483
.3048	10000	429.80	33.2	4.48	.000198	386.64	19.0	4.67	.000418
1.0000	1	.85	17.4	2.05	.000092	.42	18.7	1.72	.000021
1.0000	3	2.68	17.4	2.58	.000309	1.48	18.7	2.26	.000077
1.0000	10	8.32	17.4	3.04	.000648	4.46	18.7	2.74	.000182
1.0000	30	19.94	17.4	3.42	.001035	9.68	18.7	3.08	.000250
1.0000	100	59.82	17.7	3.90	.002061	33.71	18.7	3.62	.000691
1.0000	300	107.00	17.7	4.13	.001852	61.75	19.0	3.88	.000642
1.0000	1000	234.24	17.7	4.49	.002061	155.79	19.0	4.28	.000928

TABLE IV Cont'd.

		Continental Model				Oceanic Model			
Altitude (km)	Yield	Amplitude (mμ)	Period (sec)	M_s	% Coupling	Amplitude	Period	M_s	% Coupling
1.0000	3000	372..28	17.7	4.69	.001472	267.59	19.0	4.50	.000715
1.0000	10000	566.60	17.7	4.87	.000874	428.85	19.0	4.72	.000495
1.8288	1	1.77	20.2	2.31	.000282	.38	17.7	1.70	.000019
1.8288	3	3.32	20.2	2.58	.000306	1.22	17.7	2.21	.000060
1.8288	10	10.78	20.2	3.09	.000796	4.18	17.7	2.74	.000180
1.8288	30	23.69	20.2	3.44	.001108	11.61	17.7	3.18	.000385
1.8288	100	68.36	22.7	3.84	.001648	30.55	22.3	3.50	.000427
1.8288	300	132.40	22.7	4.13	.001741	69.30	22.3	3.86	.000594
1.8288	1000	256.80	22.7	4.42	.001588	172.62	22.3	4.25	.000842
1.8288	3000	436.88	22.7	4.65	.001272	319.93	33.2	4.35	.000403
1.8288	10000	600.70	22.7	4.70	.000691	599.69	33.2	4.62	.000342
3.6576	1	.97	17.4	2.11	.000119	.51	27.5	1.64	.000014
3.6576	3	2.52	17.4	2.52	.000240	1.43	28.1	2.07	.000083
3.6576	10	8.30	17.4	3.04	.000646	4.62	28.1	2.58	.000091
3.6576	30	28.49	17.4	3.44	.001086	13.91	28.1	3.06	.000230
3.6576	100	42.28	17.4	3.75	.001159	37.77	28.1	3.49	.000411
3.6576	300	96.46	17.7	4.10	.001554	95.36	28.1	3.90	.000687
3.6576	1000	153.48	17.7	4.30	.001019	230.80	28.1	4.28	.000925

TABLE IV Cont'd.

		Continental Model				Oceanic Model			
Altitude (km)	Yield	Amplitude (mμ	Period (sec)	M_s	% Coupling	Amplitude	Period	M_s	% Coupling
3.6576	3000	308.00	46.5	4.19	.000215	441.20	28.1	4.56	.008906
3.6576	10000	579.60	46.5	4.46	.000186	841.50	28.1	4.84	.000780
4.8768	1	1.08	22.3	2.05	.000091	.45	18.7	1.74	.000023
4.8768	3	3.44	22.3	2.55	.000272	1.48	18.7	2.26	.000077
4.8768	10	9.71	22.3	3.00	.000550	4.11	19.0	2.70	.000153
4.8768	30	22.37	22.3	3.37	.000821	11.27	19.0	3.14	.000321
4.8768	100	68.18	22.7	3.79	.001354	29.48	29.4	3.36	.000244
4.8768	300	95.56	22.7	3.99	.001080	71.87	29.4	3.75	.008390
4.8768	1000	211.50	22.7	4.34	.001149	190.80	29.4	4.18	.000623
4.8768	3000	326.10	44.9	4.23	.000251	364.00	29.4	4.46	.000612
4.8768	10000	622.00	44.9	4.51	.000221	604.60	38.2	4.56	.000276
10.0000	1	.94	24.9	1.94	.000057	.63	17.7	1.92	.000051
10.0000	3	2.58	24.9	2.38	.000129	1.87	17.7	2.39	.000134
10.0000	10	6.42	24.9	2.78	.000211	4.55	17.7	2.78	.000211
10.0000	30	13.78	24.9	3.11	.000283	11.26	17.7	3.17	.000364
10.0000	100	32.29	24.9	3.68	.000388	29.94	17.7	3.59	.000620
10.0000	300	67.71	46.5	3.53	.000158	69.71	38.2	3.63	.000235
10.0000	1000	146.50	46.5	3.86	.000182	133.28	38.2	3.91	.000216

TABLE IV Cont'd.

		Continental Model				Oceanic Model			
Altitude (km)	Yield	Amplitude (mμ)	Period (sec)	M_s	% Coupling	Amplitude	Period	M_s	% Coupling
10.0000	3000	276.60	46.5	4.14	.000179	268.40	38.2	4.21	.000238
10.0000	10000	446.10	46.5	4.35	.000120	462.80	38.2	4.45	.000177
18.6000	1	3.33	22.3	2.54	.000768	1.04	22.7	2.03	.000082
18.6000	3	8.39	22.3	2.94	.001406	2.73	22.7	2.45	.000171
18.6000	10	20.18	22.3	3.32	.002050	7.67	23.7	2.89	.000347
18.6000	30	35.58	22.3	3.57	.001863	18.96	35.1	3.10	.000271
18.6000	100	64.09	22.7	3.82	.001510	35.48	35.1	3.37	.000249
18.6000	300	108.50	22.7	4.05	.001242	82.53	46.5	3.60	.000214
18.6000	1000	180.48	22.7	4.27	.000880	152.40	46.5	3.88	.000194
18.6000	3000	270.00	22.7	4.44	.000575	220.00	46.5	4.04	.000121
18.6000	10000	408.60	22.7	4.62	.000342	336.30	46.5	4.22	.000075
30.7000	1	5.15	17.7	2.83	.002639	1.91	31.6	2.15	.000188
30.7000	3	10.77	17.7	3.15	.003363	4.26	31.6	2.49	.000210
30.7000	10	20.55	19.8	3.38	.002598	11.51	31.6	2.93	.000396
30.7000	30	31.20	19.8	3.56	.001809	25.82	32.4	3.27	.000543
30.7000	100	52.00	20.2	3.78	.001287	47.20	32.4	3.53	.008475
30.7000	300	82.52	20.2	3.98	.000950	72.62	32.4	3.72	.000336
30.7000	1000	129.00	20.2	4.17	.000609	126.00	32.4	3.95	.000261

TABLE IV Cont'd.

Altitude (km)	Yield	Continental Model				Oceanic Model			
		Amplitude (mμ)	Period (Sec)	M_s	% Coupling	Amplitude	Period	M_s	% Coupling
30.7000	3000	188.70	20.2	4.34	.000385	198.40	32.4	4.15	.000188
30.7000	10000	282.70	20.2	4.51	.000226	316.90	32.4	4.36	.000124
51.2000	1	5.13	22.7	2.72	.001656	5.69	22.7	2.76	.002005
51.2000	3	8.58	22.7	2.94	.001418	10.86	22.7	3.05	.002176
51.2000	10	14.79	22.7	3.18	.001140	20.56	22.7	3.32	.002064
51.2000	30	23.51	22.7	3.38	.000869	28.54	22.7	3.47	.001225
51.2000	100	36.92	22.7	3.58	.000578	49.21	22.7	3.70	.008965
51.2000	300	54.30	22.7	3.74	.000378	71.56	22.7	3.86	.000609
51.2000	1000	81.72	22.7	3.92	.000229	102.20	22.7	4.02	.000336
51.2000	3000	118.00	22.7	4.08	.000143	156.60	22.7	4.20	.000231
51.2000	10000	176.20	22.7	4.26	.000085	241.10	22.7	4.39	.000143
66.0000	1	4.24	17.7	2.75	.001844	3.83	19.0	2.67	.001338
66.0000	3	6.43	17.7	2.93	.001321	5.84	19.0	2.85	.000921
66.0000	10	9.79	17.7	3.11	.000850	9.37	19.0	3.06	.000690
66.0000	30	14.16	17.7	3.27	.000349	13.72	19.0	3.22	.000457
66.0000	100	21.43	17.7	3.45	.000344	20.31	19.0	3.39	.000276
66.0000	300	31.16	17.7	3.61	.000222	28.84	19.0	3.55	.000191
66.0000	1000	46.76	17.7	3.79	.000135	42.36	19.0	3.71	.000100

TABLE IV Cont'd

Altitude (km)	Yield	Continental Model				Oceanic Model			
		Amplitude (mμ)	Period (sec)	M_s	% Coupling	Amplitude	Period	M_s	% Coupling
66.0000	3000	67.60	17.7	3.95	.000085	68.34	19.0	3.87	.000062
66.0000	10000	101.10	17.7	4.12	.000050	89.19	19.0	4.04	.0000066
80.0000	1	3.12	20.2	2.55	.000818	2.53	27.5	2.33	.000309
80.0000	3	4.60	20.2	2.72	.000559	3.72	27.5	2.50	.000212
80.0000	10	6.94	20.2	2.90	.000358	5.56	27.5	2.67	.000164
80.0000	30	18.05	20.2	3.06	.000234	7.97	27.5	2.83	.000087
80.0000	100	15.05	20.2	3.24	.000145	11.81	27.5	3.00	.000053
80.0000	300	21.73	20.2	3.40	.000093	16.92	27.5	3.15	.000084
80.0000	1000	32.47	20.2	3.57	.000057	25.13	27.5	3.33	.000021
80.0000	3000	46.83	20.2	3.73	.000036	36.11	27.5	3.48	.000013
80.0000	10000	69.97	20.2	3.91	.000021	53.79	27.5	3.66	.000008

APPENDIX A

Disc pressure source

Our assumed pressure source is constant over a disc of radius a, and with a transformed time history $B(\omega)$, i.e.,

$$\langle p_s(r,\theta)\rangle = \begin{cases} B(\omega), & r<a \\ \\ o\ , & r>a \end{cases} \qquad \text{(A-1)}$$

Using the area integration technique, we obtain

$$\langle w\ (r,\theta)\rangle = B(\omega) \int_o^{2\pi} \int_o^a G(\underset{\sim}{r}|\underset{\sim}{r}_o)\ r_o\, dr_o\, d\theta_o$$

$$= \frac{-i}{2\pi} B(\omega) \int_o^{\infty} \frac{[GN - LH]}{F_R} \int_o^{2\pi} \int_o^a J_o(kR) r_o \quad dr_o\, d\theta_o$$

where

$$R^2 = r_o^2 + r^2 - 2rr_o \cos(\theta-\theta_o)$$

From the addition theorem of Bessel functions,

$$J_o(kR) = \sum_{m=o}^{\infty} \varepsilon_m J_m(kr_o)\ J_m(kr)\ \cos(m(\theta-\theta_o))$$

where the Neuman factor ε_m is defined as

$$\varepsilon_m = \begin{cases} 1, & m = o \\ 2, & m \neq o \end{cases}$$

Since

$$\cos[m(\theta-\theta_o)] = \cos(m\theta)\cos(m\theta_o) - \sin(m\theta)\sin(m\theta_o)$$

the integration over θ yields

$$\langle w(r,\theta)\rangle = -iB(\omega) \int_o^\infty \frac{[GN - LH]}{F_R} J_o(kr) \int_o^a J_o(kr) r_o \, dr_o \, dk$$

where we have used the relations

$$\int_o^{2\pi} \cos(m\theta)\, d\theta = \begin{cases} o, & m \neq o \\ 2\pi, & m = o \end{cases}$$

and

$$\int_o^{2\pi} \sin(m\theta)\, d\theta = o \text{ for all } m.$$

Since

$$\int_0^a J_o(kr_o) r_o \, dr_o = \frac{a}{k} J_1(ka)$$

our solution for the disc source is:

$$\langle w_o(r,\theta) \rangle = -iB(\omega)a \int_o^\infty \frac{[GN - LH]}{F_R} \frac{J_1(ka)}{k} J_o(kr) \, dk \qquad \text{(A-2)}$$

This solution can be verified using equations (4) and (9). The disc source can be expressed in integral form as

$$\langle p_s(r,\theta) \rangle = B(\omega)a \int_o^\infty J_1(ka) \, J_o(kr) \, dk$$

and comparison with equation (4) implies that

$$P_s = B(\omega) \, a \, J_1(ka)$$

which substituted in equation (9) gives the same result as equation (A-2).

ACKNOWLEDGMENTS

We thank Allen D. Pierce of the Massachusetts Institute of Technology and Brian L. Murphy of Mt. Auburn Research Associates for useful discussions. This research was sponsored by the Advanced Research Projects Agency under Project Vela Hotel, and monitored by the Air Force Office of Scientific Research under contract F-44620-69-C-0082 with Teledyne Geotech and contract F-44620-70-C-0120 with the California Institute of Technology

David G. Harkrider

Seismological Laboratory

California Institute of Technology

Pasadena, California 91109

Carl A. Newton* and Edward A. Flinn

Alexandria Laboratories

Teledyne Geotech

Alexandria, Virginia 22314

*Present address: Seismological Laboratory, California Institute of Technology, Pasadena, California